



MONTCLAIR STATE
UNIVERSITY

Montclair State University
**Montclair State University Digital
Commons**

Theses, Dissertations and Culminating Projects

5-2017

Targeting SAV Restoration at Lake Mattamuskeet Using GIS and Landsat 8 Data

Lindsey Shanks
Montclair State University

Follow this and additional works at: <https://digitalcommons.montclair.edu/etd>



Part of the [Earth Sciences Commons](#), and the [Environmental Sciences Commons](#)

Recommended Citation

Shanks, Lindsey, "Targeting SAV Restoration at Lake Mattamuskeet Using GIS and Landsat 8 Data" (2017). *Theses, Dissertations and Culminating Projects*. 607.
<https://digitalcommons.montclair.edu/etd/607>

This Thesis is brought to you for free and open access by Montclair State University Digital Commons. It has been accepted for inclusion in Theses, Dissertations and Culminating Projects by an authorized administrator of Montclair State University Digital Commons. For more information, please contact digitalcommons@montclair.edu.

Abstract

Lake Mattamuskeet, a large, shallow lake on the coast of North Carolina, has undergone water quality degradation and submerged aquatic vegetation (SAV) decline over recent years. Water depth and water clarity have been established as key drivers of SAV loss. To target locations for the restoration of SAV in the lake, an analysis that focuses on water clarity, water depth, and current SAV presence was developed. Two separate methodologies were conducted and compared to analyze water clarity in the lake. The first applied four years (2013-2016) of Landsat 8 imagery to a previously developed model that predicts water clarity from the imagery. The second applied multiple interpolation techniques to data from surveys performed by the US Fish and Wildlife Service (FWS) during the years 2013-2016. The remote sensing model output was corrected for low model predictions and sun glint may have impacted results, so despite the better seasonal and temporal resolution of the remote sensing methodology, the interpolation methodology was deemed the better approach. The Empirical Bayesian Kriging interpolation technique was named the best overall approach to interpolate SAV presence and water clarity for Lake Mattamuskeet. A bathymetric map of the lake and water level data was used to estimate average water level during the SAV growing season (April-September). SAV habitat is located along the southern and eastern edges of the lake per both methodological approaches. Varying the model's initial conditions produced similar results in both cases. Increasing water depth decreased available SAV habitat, and decreasing water depth increased available SAV habitat. These results suggest that sea level rise may drive future SAV decline. Managing lake levels may be necessary to retain suitable SAV habitat and promote clear water conditions in the future.

MONTCLAIR STATE UNIVERSITY

/ Targeting SAV Restoration at Lake Mattamuskeet Using GIS and Landsat 8 Data /

By

Lindsey Shanks

A Master's Thesis Submitted to the Faculty of

Montclair State University

In Partial Fulfillment of the Requirements

For the Degree of

Master of Science in Geoscience

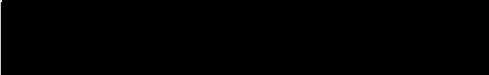
May 2017

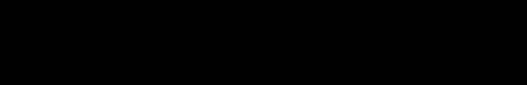
College of Science and Mathematics

Thesis Committee:

Department of Earth and Environmental Studies


Dr. Josh Galster
Thesis Sponsor


Dr. Mark Chopping
Committee Member


Dr. Danlin Yu
Committee Member

**TARGETING SAV RESTORATION AT LAKE MATTAMUSKEET
USING GIS AND LANDSAT 8 DATA**

A THESIS

**Submitted in partial fulfillment of the requirements
For the degree of Master of Science in Geoscience**

By

LINDSEY SHANKS

Montclair State University

Montclair, NJ

2017

Table of Contents

Introduction.....	1
Methods.....	8
Results.....	14
Discussion.....	17
Conclusion.....	23
References.....	24

Tables

Table 1. Landsat 8 Bands (modified from USGS 2016a)	29
Table 2. Band Combinations Tested (from Ozen et al. 2016a)	30
Table 3. Dates of Available Landsat 8 Imagery.....	31
Table 4. Landsat 8 Images Chosen for Analysis.....	32
Table 5. Summary of SAV Survey Data.....	33
Table 6. Interpolation Comparison.....	34

Figures

Figure 1. Secchi Disk (from Maryland Department of the Environment 2017) ...	35
Figure 2. Landsat History (from USGS 2016b)	36
Figure 3. Study Site.....	37
Figure 4. SAV Decline (from Moorman et al. <i>in press</i>).....	38
Figure 5. Location of USGS Monitoring Stations (from USGS 2016c)	39
Figure 6. Landsat Scene and Subset.....	40
Figure 7. Preliminary SAV Habitat Analysis.....	41
Figure 8. Modeled Water Clarity: East.....	42

Figure 9. Modeled Water Clarity: West.....	43
Figure 10. Validation of Water Clarity East Model.....	44
Figure 11. SAV Presence Interpolation.....	45
Figure 12. Water Clarity Interpolations.....	46
Figure 13. Method Comparison.....	47
Figure 14. Water Clarity Averages	48
Figure 15. Target SAV Restoration Locations, Remote Sensing Methodology ...	49
Table 16. Target SAV Restoration Locations, Interpolation Methodology.....	50
Figure 17. Initial Condition Variations, Remote Sensing Methodology.....	51
Figure 18. Initial Condition Variations, Interpolation Methodology.....	52
Figure 19. Near-Infrared Band of Images After Histogram Matching.....	53
Figure 20. Examples of Sun Glint (from Kay et al. 2009)	54
Figure 21. Turbidity Trend in Lake Mattamuskeet (from USGS 2016c)	55
Figure 22. High Variability of Water Clarity (from Google Earth 2017)	56

Introduction

Submerged aquatic vegetation (SAV) is a crucial part of aquatic ecosystems (Burkholder et al. 2007). SAV provides food and habitat for many species, traps and stabilizes sediment leading to higher water clarity, and takes up excess nutrients and pollutants, preventing eutrophication and improving overall water quality. SAV also influences water flow and stores carbon. Decline of SAV has been observed worldwide and because of the ecological services it provides, restoration of SAV can be critical to reestablishing degraded aquatic ecosystems (Orth et al. 2006).

Declines in SAV may be particularly detrimental for shallow lakes. According to the concept of alternative stable equilibria (Scheffer et al. 1993), shallow lakes are thought to stabilize in either a clear, macrophyte-dominated state or a turbid, phytoplankton-dominated state. A shift from one state to the other is generally rapid and thought to require a significant perturbation. Jeppeson et al. (2007), however, later suggested that the alternative states are less stable than previously thought, but noted that even upon improved water clarity conditions, SAV restoration may still be necessary to maintain clear conditions. Therefore, whether the stable state hypothesis holds or not, restoration of SAV in degraded shallow lakes could be crucial for the reestablishment of clear conditions in shallow lake ecosystems.

Knowledge of the spatial distribution of SAV as well as related water quality parameters is necessary for restoration efforts. Successive mapping of SAV presence over time is a useful way to observe and analyze SAV decline. Approaches to SAV presence mapping range from field surveys (Harwell et al. 2009, Cho and Poirrier 2005) to using remotely sensed imagery (Dhillon et al. 2014, Zou et al. 2013, Zhang et al. 2016). Water

quality and other environmental variables can be mapped along with SAV presence to understand the drivers of SAV decline and to predict future habitat changes. Field-obtained environmental measurements can be interpolated to produce continuous maps from a limited number of observations.

Different interpolation techniques exist to determine values for areas that were not directly sampled. The Inverse Distance Weighed (IDW) technique has been applied to water quality variables (Xu et al. 2001), and variations of the Kriging technique have been applied in similar analyses (Audu and Usman 2015, Dhillon et al. 2014). IDW is a deterministic method for spatial interpolation, while Kriging is stochastic. The IDW technique requires the assumption presented in Tobler's First Law of Geography (Tobler 1970), that closer objects have more in common than objects further away, because it bases predictions on surrounding measurements. Measurements further away from the prediction area have less influence than nearby measurements. IDW has been compared to Kriging extensively in the literature (Murphy et al. 2010, Mueller et al. 2004, Zimmerman et al. 1999).

Like IDW, Kriging weighs the surrounding measurements to create predictions. Unlike IDW, the Kriging method is based on the statistical relationships among the measured points. The method assumes that the distance between points reflects a spatial correlation. The data must first be fitted to a semivariogram model before the data are interpolated. One variation of the Kriging technique, called Empirical Bayesian Kriging (EBK), accounts for the uncertainty in these predictions.

For the Kriging method, parameters must be manually selected. EBK automatically calculates parameters through a process of simulations. It also accounts for

the error that comes from estimating the semivariogram. While most Kriging methods calculate the semivariogram from measurements and use the single semivariogram for the interpolation, for EBK, a semivariogram is estimated for a subset of data and then new data is simulated at each measurement point in the subset. From the simulated data, a new semivariogram is estimated and the process is repeated for a specified number of times. The process creates many semivariograms for each subset, or a distribution of semivariograms, and the empirical semivariances can be determined. The EBK method is advantageous because the standard errors of prediction are more accurate than for other Kriging methods, and it is more accurate for smaller datasets. The primary disadvantage of the method is the long processing time (Pilz and Spock 2007).

Water quality maps are required for habitat suitability analysis, which utilizes information about the spatial distribution of different environmental factors to determine whether areas are suitable for the growth of particular species. SAV habitat suitability analysis requires current presence/absence data along with other data relevant to the abundance of SAV, including water clarity and water depth. Water clarity and depth have been identified as the two most important determinants of SAV presence (Zhang et al. 2016). The two parameters have been used in previous SAV habitat suitability analyses (Havens et al. 2003, Poirrier et al. 2009), and it has been recommended that having higher resolution bathymetry and light climate data would improve model results (Harwell et al. 2009). The call for more detail regarding these two parameters highlights their importance in determining SAV habitat suitability.

Water clarity is a measurement of the total constituents in the water column, and is determined by how clear, or transparent, the water column appears to be. Clarity can be

measured in several ways, but one of the most common and easiest is using a Secchi disk (Figure 1). The Secchi disk is a 20-centimeter black and white disk that is inserted into the water, and the maximum depth at which the disk is visible is known as the Secchi disk depth (SDD) or Secchi disk transparency (SDT). The SDD/SDT is approximately equal to one half of the photic zone, the depth that light will penetrate to. Decreases in water clarity can be caused by anything that impacts the ability of light to penetrate the water column, such as increasing abundance of phytoplankton, typically in response to excess nutrients, or by a storm event that increases turbidity. Seer and Shears (2015) found that turbidity varies highly month-to-month, and explanatory environmental variables are different in different regions. Therefore, site-specific information (both spatial and temporal) must be considered to define accurate water clarity conditions for any particular site.

The measurement of water clarity is one of the many applications of remote sensing to hydrologic research and has been widely explored in the literature (Nelson et al. 2003, Wu et al. 2009, Butt and Nazeer 2015). Jensen (2010) provides essential background for the understanding of remotely sensed water clarity. Remote sensing of turbidity requires *in situ* measurements and the selection of an appropriate remote sensing metric to calibrate remotely sensed data. Field measurements should be taken on days with little wind, because wind causes additional specular reflection towards the sensor due to wave action on the surface. The spectral reflectance of suspended sediment depends on both the amount of material and the characteristics of the material, such as size and absorption. For water with suspended minerals in the water column, the peak reflectance shifts toward longer wavelengths in the visible spectrum. The visible

wavelength range of 580-680 nm may be useful to distinguish the type of suspended sediments, and the near-infrared wavelength range of 713-880 nm could inform the amount of suspended minerals (Jensen 2010).

Algal plant organisms contain chlorophyll *a* pigment, which also changes the spectral reflectance characteristics of pure water. Chlorophyll *a* produces strong absorption of blue light between 400-500 nm and red light at approximately 675 nm, with a reflectance maximum around 550 nm because of relatively lower absorption of green light, and a peak around 690-700 nm. Essentially, the presence of chlorophyll *a* in the water column decreases the amount of reflectance in the blue and red wavelengths and increases in the green wavelengths. When turbidity and chlorophyll are both present, a different response occurs. It is typically difficult to differentiate chlorophyll *a* from dissolved organic matter in coastal and inland surface waters (Jensen 2010).

A range of satellites have been used to measure water clarity including IKONOS, QuickBird, SPOT, SeaWiFS, MERIS, MODIS, and Landsat (Ozen et al. 2016b). Landsat is advantageous because the Landsat program has collected the longest consecutive span of Earth observing imagery, beginning in 1972 (Figure 2), and level-1 standard products are available at no cost (USGS 2016a). The Landsat 8 spacecraft, launched in 2013, carries two sensors: the Operational Land Imager (OLI) and the Thermal Infrared Sensor (TIRS). The OLI measures visible, near-infrared and shortwave infrared reflectance with 30-meter multispectral spatial and 15-meter panchromatic resolutions. The sensor is a “push-broom” design. It uses long linear detector arrays with thousands of detectors per spectral band. This is a significant improvement over previous sensors that used oscillating mirrors to sweep the field of view across the swath, known as “whiskbroom.”

The satellite travels a sixteen-day repeat cycle in a heliosynchronous orbit that ensures observations are made at the same local solar time for each location. Landsat 8 has 11 bands (Table 1). Bands 2, 3, and 5, which are most important to this study, are visible blue, green, and near infrared, respectively. The images are radiometrically and geometrically corrected. The data is corrected for view angle effects, satellite distortions including altitude deviations, and Earth distortions like rotation, curvature, and relief. Relative detector differences and dark current bias are removed. The products are provided in digital number (DN) units, which can then be converted to spectral radiance, top of atmosphere (TOA) reflectance, or surface reflectance (USGS 2016a).

Landsat imagery has been used in many studies to estimate lake clarity using regression analysis to correlate Landsat data and ground observations (Butt and Nazeer 2015, Nelson et al. 2003, Kloiber et al. 2002). Coefficients in the regression equation are expected to be consistent with factors unique to a specific scene. Ideally, a single equation with constant coefficient values can be used to calculate a water clarity index that could be applied to many images in the region over a large temporal scale. This would minimize the need for ground data to calibrate the remotely sensed data, which would be very useful in water clarity monitoring because field sampling is time intensive, and ground data used for calibration of satellite data is limited by a time window due to the temporal variability of water clarity (Kloiber et al. 2002). Kloiber et al. (2002) analyzed the possibility of using a single, constant-form equation to relate field observations and satellite data to allow for comparison across images. Kloiber et al. (2002) concluded that a consistent band combination, blue / red + blue could be applied for images over a 25-year period in Minnesota, suggesting that for a constant scene, the

same band combinations can be used to predict water clarity across time without *in situ* calibration data for every image. This has been found in studies between SSD and Landsat data involving only a few lakes to regional analysis, as was this study (Kloiber et al. 2002).

A recent study performed by Ozen et al. (2016a) in conjunction with the U.S. Fish & Wildlife Service at the Mattamuskeet National Wildlife Refuge investigated whether satellite imagery could be used to monitor water clarity at Lake Mattamuskeet. The study analyzed a 16-bit Landsat 8 scene with DN values from March 2013 and made use of a limited amount of SDD data. Due to a hydrological disconnect between the east and west basins of the lake as described by Waters et al. (2010), the east and the west sides were modeled separately in this study. A single dataset containing 15 measurements on the east side of the lake and 15 measurements on the west side of the lake was found in which the survey date corresponded to +/- 1 day from the Landsat scene. Nine pixel values from the Landsat image at each measurement point were extracted and averaged and used for regression modeling to establish a relationship between the field measurements and remotely sensed data.

Previous work that determined water clarity from satellite imagery was reviewed, and all the band combinations that were used in previous research were tested (Table 2) in Ozen et al. (2016a). A total of 42 variations of bands and band combinations were applied. It was determined that different band combinations produced the most statistically significant relationship for the two basins of the lake ($p < 0.05$). For the most accurate results determined by running Akaike's information criteria (AIC), the east side required the combination of the blue and NIR bands, while the west side required the

blue, green, and NIR bands ($R^2=0.83$ and $R^2=0.59$, respectively). It was suggested that this difference might be influenced by the differences in depth on the two sides of the lake, although the biophysical communities differ as well. The final equations are:

$$SDD_{\text{east}} = 1.14 - 0.00011 \times (\text{blue}) - 0.0000055 \times (\text{NIR}) \quad \text{Eq. (1)}$$

$$SDD_{\text{west}} = 4.70 - 0.001 \times (\text{blue}) + 0.00026 \times (\text{green}) + 0.00034 \times (\text{NIR}) \quad \text{Eq. (2)}$$

The purpose of this study is to answer the question: in which areas of Lake Mattamuskeet should we focus SAV restoration efforts? In the process of answering this question, two methods for estimating water clarity are compared: modeling from Landsat 8 data and interpolating from field measurements. Multiple interpolation techniques are tested and compared. Water clarity information from both methodologies, a bathymetric map and lake level data to inform water depth, and the most recent SAV presence survey are used to assess the lake for potential SAV habitat under current conditions as well as for some possible future scenarios.

Methods

Study Site

Lake Mattamuskeet (Figure 3) is located along the Atlantic Flyway, making it a vital stopover for more than 200,000 wintering waterfowl annually. It is the largest natural lake in North Carolina, and the hydrology has been drastically altered by several changes to the lake and surrounding watershed. The first of four drainage canals that connect the lake to the Pamlico Sound was constructed in 1850, reducing the lake's 3-meter depth to its current 1-meter average. The lake was drained three times and the

drained lake bottom farmed twice between 1915-1932 with the assistance of pumps that were once capable of draining the lake. Today, about 162 km² of open water remain, surrounded by cropland and a complex network of canals and pumps. Due to the low relief of the watershed, the surrounding Coastal Plain, and its proximity to the ocean, the hydrology is controlled largely by pumping. Farmers continue to pump in the area not only to maintain cropland, but also to flood and drain impoundments, sometimes multiple times per season. Impoundments are managed areas that are drained in the summer to grow vegetation that attracts ducks and other waterfowl, and flooded in the winter to attract the wildlife. Much of the drained water works its way through the canal system into Lake Mattamuskeet, bringing large amounts of sediment and nutrients into the lake. An agreement upon the establishment of Mattamuskeet National Wildlife Refuge allows neighboring landowners to continue pumping into the lake (Winton et al. 2016, Motorman et al. *in press*).

Although Lake Mattamuskeet is not adjacent to the coast with a direct threat from sea level rise, four drainage canals hydrologically connect it to the Pamlico Sound, which is currently experiencing sea level rise at an average rate of 3 mm/year (NC Coastal Resource Commission 2015). When the national wildlife refuge was established, water control structures were built across the four main canals that connect the lake to the Sound to prevent saltwater intrusion. These structures open when lake levels are higher than the Sound levels, allowing the lake water to drain into the Sound. When Sound levels are higher, the structures remain shut, preventing saltwater from entering the lake. Sea level rise will cause the water level in the Sound to remain higher for longer periods of time, so the structures will remain closed for longer, forcing lake level to remain

higher as well. Although the surrounding lake topography may limit the level to which the water can rise, scenarios in which the lake level has increased due to sea level rise are likely in the future.

The lake is divided into two basins (Figure 3) by a highway that was constructed in 1940 and five culverts connect the two sides of the lake (Waters et al. 2010). In the mid-1990s, SAV on the west side of the lake began to decline and is now entirely absent. The east side of the lake began to follow the trend in 2013 (Figure 4). SAV loss followed a severe decrease in water quality, particularly water clarity (Moorman et al. *in press*). Management plans to restore SAV are already in consideration. However, a better understanding of the area's hydrology and the drivers of water quality, particularly water clarity, could provide essential insight to restoration plans.

Field data

A gridded sampling approach was used for SAV surveys performed during the years 1989-2004 by the U.S. Fish and Wildlife Service (FWS). Surveys were performed using a transect sampling approach (104 points across 7 transects) in 2013, 2014, and 2015. In 2016, a new grid method was developed to account for some gaps left by the transect method. SAV surveys between 2013-2016 included percent and type of SAV, sediment type, water depth, muck depth, temperature, turbidity, conductance, pH, dissolved oxygen, and Secchi depth at each survey point.

Water level in the east and west basin has been measured daily by two USGS monitors in the lake since 2015 (Figure 5). Data from these monitors is publicly available from the USGS (<https://nc.water.usgs.gov/projects/mattamuskeet/data.html>). Wind speed

and direction data was obtained from Weather Underground (<https://www.wunderground.com/>).

Remotely Sensed Data

Landsat 8 imagery was obtained from the USGS Earth Explorer website (<https://earthexplorer.usgs.gov>). All available, cloud-free data for the study site (path 35, row 14) was downloaded (shaded cells in Table 3). Each 16-bit image was provided in GeoTIFF format in the UTM Zone 18 projection in DN units. Data representative of each seasonal period was selected from available data from 2013-2016 (Table 4). Selected datasets were processed using ERDAS Imagine 2015. Using the batch command, the GeoTIFF files for bands 2, 3 and 5 were imported as Imagine images. Due to the large size of the Landsat images, images were subset to the size of the study area (24km by 15km, 800 pixels by 500 pixels) during the import process (Figure 6).

To use the same equation for multiple Landsat scenes over time, correction was required to prevent atmospheric differences from overshadowing actual changes (Goslee 2011). Histogram Matching was used to normalize images so that the equation developed for the April 2013 scenes could be applied to scenes from the fifteen additional dates selected for this study. Areas of interest (AOIs) were developed for all the water pixels in the east and west sides of the lake. For the entire lake AOI, the histogram of each required scene was matched to the April 2013 scene for each band required by the equations.

The model maker was used to apply Equations 1 and 2 to the normalized images for the east and west sides of Lake Mattamuskeet, respectively. The model was run for each of the sixteen selected images. To assess the success of this model, a field dataset

collected within five days of the Landsat scene on July 19, 2013, was used. Modeled values were extracted at each sampling point and a measured vs. modeled plot was created. Small predicted SDD values that appeared to be influenced by sun glint were omitted from the model results. Sun glint occurs due to specular reflection, when waves reflect light directly back toward the sensor (Kay et al. 2009).

Interpolations

Ordinary Kriging, Empirical Bayesian Kriging (EBK), Inverse Distance Weighed (IDW), and global polynomial interpolation (GPI) techniques were applied and evaluated with leave-one-out cross validation using the ESRI geostatistical analyst. IDW was performed with powers 1, 2, and 3, and EBK was performed with a power semivariogram, a linear semivariogram, and a thin plate spline semivariogram. GPI was performed with a first-, second-, and third-order polynomial. The interpolation technique that produced the lowest root mean squared error (RMSE) was chosen as the best-performing interpolation for this data.

Habitat Suitability Analysis: Preliminary

A simple, preliminary habitat suitability analysis was performed using ESRI ArcMap for a binary raster analysis. Water clarity and water level were most related to SAV presence and deemed vital to SAV decline in the literature (Moorman et al. *in press*, Zhang et al. 2016, Harwell et al. 2009, Poirrier et al. 2009, Havens et al. 2003), so clarity, water level, and SAV presence were used in the analysis. The 2016 SAV survey dataset (closest to current conditions) was initially used to create interpolations for each variable. Each raster was reclassified based on clarity, water level, and SAV presence during the years 2013-2015. Water levels and clarities in which SAV was present in the past (all

water levels less than 1.04 meters, and all SDDs greater than 0.15 meters), as well as SAV presence ranging from 1-100%, were reclassified to 1. All other depths, SDDs, and 0% SAV presence were set to zero. The analysis applied a simple formula ensuring that if a single condition failed, the area would be deemed unsuitable:

$$\text{habitat} = \text{depth} \times \text{clarity} \times \text{cover}$$

A scenario to capture the possible effects of sea level rise was simulated by increasing initial water level by 0.1 meters. Water level was then increased further to determine the amount of water level increase due to sea level rise that would have to occur to produce a negligible amount of remaining SAV habitat (Figure 7). Currently, water levels are not actively managed at Lake Mattamuskeet; the water control structures open and close entirely based on water level. Refuge staff cannot force them to close or remain open for extended periods, but a potential scenario reflecting water level management was represented by decreasing water depth by 0.1 meters.

Habitat Suitability Analysis: Final

Two SAV habitat suitability analyses with a better representation of clarity and depth fluctuations were produced and compared. One applied water clarity model results from the remote sensing methodology, and one applied water clarity from interpolated field measurements. A single raster dataset for clarity was prepared by averaging the best interpolations from each year, selected based on the lowest RMSE produced during leave-one-out cross validation. Due to a lack of SDD measurements taken during 2013, producing highly variable interpolation results, 2013 SDD was omitted. A similar single raster dataset was also produced from the remote sensing methodology by taking the average of the model output for summer 2014-2016 results.

Average water level during the SAV growing season (April-September) was calculated from daily USGS lake level data and a bathymetric map developed by the USFWS was used to produce a raster dataset for water level. The best interpolation of the SAV presence dataset was also selected.

The water clarity, water level, and SAV presence rasters were reclassified using a new classification. Chesapeake Bay water quality standards were consulted (Tango and Batiuk 2013) due to similarities between the two water bodies, but it was determined that reclassifying based on these standards did not produce suitable SAV habitat. Instead, the SAV surveys were analyzed to determine average water clarity in locations only where SAV was present over the past four years. An average was used because of the high variability of water clarity. For depth, which also varies but is more consistent overall, the maximum depth at which SAV was 100% present over the past four years was used for reclassification. Suitable conditions were assigned a value of 1, and unsuitable conditions were assigned a value of 0. Reclassified rasters were applied to the equation:

$$\text{habitat} = \text{depth} + \text{clarity} + \text{cover}$$

This equation produced a range from zero to three, representing the least to the most suitable locations for SAV restoration.

Results

Multiple outputs were produced in the process of targeting locations for SAV restoration in the lake. Water clarity was analyzed first using Landsat 8 imagery to study seasonal changes over a four-year period. Water clarity was also analyzed by interpolating field measurements taken during the summer of the same four years. Various interpolation techniques were compared to determine the best interpolation

method for water clarity data. SAV presence was also interpolated from field measurements. The analysis to target locations for SAV restoration was performed twice, once using water clarity results from the remote sensing methodology and once using water clarity results from the interpolations of filed measurements.

Remote Sensing

A total of 32 raster datasets (16 for each side of the lake) spanning from April 2013 – December 2016 were produced to model water clarity during different seasons of the four-year period (Figures 8-9). A distinct linear pattern appears on most of the output imagery that corresponds with the prevailing wind direction during the time the image was captured. Both models produced values below zero in the areas of the lake where the linear pattern was most prevalent. For the east side, this occurred predominately during spring and summer scenes. For the west side, these values dominated large portions of the lake for most of the scenes.

One dataset was available to validate the model results, separate from the *in-situ* dataset and Landsat scene upon which the model was developed (April 14, 2013). A dataset composed of *in-situ* measurements collected in July 2013 in the east side of the lake was compared to the results derived from the July 19, 2013 Landsat scene. The model under-predicted SDD for this date ($r^2=0.586$; Figure 10). There were no other surveys that corresponded to a Landsat scene for this analysis with enough field measurements to provide further validation.

Interpolations

Based on RMSE calculated during cross validation for each interpolation, EBK outperformed the other interpolation techniques for SAV presence and for water clarity in

2015 and 2016 (Table 6). The power semivariogram produced the best EBK interpolation for every dataset. For water clarity in 2014, the second-order global polynomial interpolation was the best technique, although the EBK technique produced the next-best result. For 2013 water clarity, IDW with a power of 1 and all global polynomial interpolations performed better than EBK. The Ordinary Kriging technique produced RMSEs slightly higher than EBK in each case.

The final SAV raster dataset, created from the EBK power semivariogram interpolation method for the 2016 data, shows that most of the lake currently lacks SAV, and most of the remaining SAV is sparse (Figure 11). The 2013 water clarity interpolation was omitted from further analysis because of the variability of interpolation results due to a smaller number of field measurements. The three best water clarity rasters, produced from the overall best-performing interpolation method for water clarity for the 2014, 2015, and 2016 datasets (EBK with a power semivariogram) suggest that clarity is variable and has generally decreased over time (Figure 12).

Water Clarity: Remote Sensing Model vs. Interpolation of Measurements

Results for SDD over the years 2013-2016 from the remote sensing analysis were compared to the best-performing interpolations of field measurements for each year (Figure 13). Initial model results were much lower than interpolations from field measurements. Because the remote sensing model produced a range of extremely low values, the result was adjusted to portray realistic values. The raster was multiplied by 3.5. This factor was determined by forcing the validation plot's trend line through the origin (Figure 10). The slope of the new line represented the factor that needed to be

applied to the model results in order to produce a 1:1 relationship with field measurements (Figure 14).

Habitat Suitability Analysis

Locations for SAV restoration were identified along the eastern and southern border of the lake, where some SAV is still present and the water is clearest and shallowest (Figures 15-16). Habitat with the best suitability is available for a total of 14.46 km² according to the remote sensing analysis and only 2.64 km² according to the interpolation analysis. For a 0.1 m increase in water level, the available SAV habitat reduces to 8.68 km² and 2.3 km² for the remote sensing and interpolation methodologies respectively (Figures 17-18). For another increase of 0.1 m, ideal habitat disappears entirely in both cases. Habitat considered “moderately” suitable, fulfilling only two of the three ideal conditions, is available for 39.61 km² and decreases to 35.87 km², 31.99 km², and 31.47 km² with incremental 0.1-m increases in water level for the remote sensing analysis. A similar decrease occurs according to the interpolation analysis: from 31.61 km² to 18.82 km², 2.99 km², and 2.64 km². For a small decrease in water level, the best possible SAV habitat only increases slightly to 17.78 km² for the remote sensing analysis and 2.64 km² for the interpolation analysis because water clarity is the limiting condition. With 0.1 m incremental decreases in water level, “moderately” suitable habitat increases from 39.61 km² to 45.31 km², 54.04 km², and 56.83 km². The same trend occurs for the interpolations analysis: 31.61 km² to 41.40 km², 53.99 km², and 63.33 km².

Discussion

SAV habitat suitability for SAV restoration was identified within Lake Mattamuskeet based on the assumptions that (1) habitat suitability is closely linked to

water depth and clarity and (2) SAV restoration will have the best chance to succeed near existing SAV. Previous studies have made similar assumptions (Harwell et al. 2009, Cho and Poirrier 2005). The assumption of these conditions allowed for a simple yet effective and straightforward analysis that has implications for SAV restoration in Lake Mattamuskeet and in other lakes experiencing SAV declines.

Remote Sensing of Water Clarity

The models used to predict SDD from Landsat 8 data at Lake Mattamuskeet were developed based on a Landsat scene and field measurements from April 2013. A comparison of field measurements to modeled SDD was performed on a scene and field measurements from the same year, but a different season (July 2013, Figure 10). Although the model captured a relationship between field measurements and model predictions ($r^2=0.586$), the modeled values were much lower than measured values, suggesting that the model was consistently producing values that were too low. One possible explanation for the model's performance is that it was developed for a dataset collected in April, and then applied to Landsat scenes from summer, fall, and winter in addition to spring. Although the model may have captured seasonal changes in water clarity, it may also have captured seasonal changes unrelated to water clarity. The development of separate models for separate seasons could solve this problem. However, additional field measurements from multiple seasons are required to test this possibility and to produce and validate separate models.

The model produced exceptionally low and negative values for large portions of the west side and smaller, more concentrated sections in the east side (red areas in Figures 8-9). These low results, particularly in the east side, seem to be caused by more

than the model's tendency to predict small values. It appears that these areas are accompanied by a linear pattern that corresponds to the ripples that would be produced by wind based on the prevailing wind direction (Figure 8). This pattern is particularly noticeable in the near-infrared (NIR) band of each scene (Figure 19). Landsat 8's band five captures the NIR portion of the spectrum. Typically, spectral reflectance in the NIR wavelength should not be observed over water because NIR light is entirely absorbed by water.

One possible explanation for the observation is that the band has captured sun glint. Sun glint is noticeable in the NIR part of the spectrum because the radiance reflected from water should be negligible, so reflectance can be attributed to sun glint (Kay et al. 2009). Kay et al. (2009) provide some examples of sun glint (Figure 20) and in a review of methods for correcting imagery for sun glint reflection, they note that for coastal images with small pixel sizes, data from the NIR band is used as an indicator for sun glint. However, for shallow water, turbid water, or water with vegetation near the surface, this assumption of negligible NIR reflectance does not necessarily hold. This form of correction, therefore, should not be applied for Lake Mattamuskeet because of its shallowness and high turbidity. Because the lake appears to be impacted by sun glint on a seasonal basis, predominantly in the spring and summer, there may be another contributor to the reflectance. However, SAV that may be close to the surface is not present in the parts of the lake that were affected, and they appear in the deeper areas of the lake. Additionally, the seasonal trend in turbidity observed in the lake, which peaks in the winter/early spring (Figure 21) does not correspond to the spring/summer peaks in

possible sun glint. Therefore, while it is possible that there is more contributing to the NIR reflectance, it is also likely that sun glint is impacting the imagery in this study.

Spatial trends and an overall temporal trend in water clarity are not clear from the model output. Perhaps additional historical data, which could be provided by previous Landsat sensors, could provide enough information to determine whether there is an overall decreasing trend in water clarity over time, as has been reported from visual observations of the lake. Spatial trends may be decipherable with further analysis of individual images with respect to water depth and wind speed and direction data, which could impact daily clarity. However, before this level of detail can be analyzed, the model performance must be improved with additional data.

Future research could attempt to calibrate the model with *in situ* data across different seasons. This requires further field sampling to obtain data from each season corresponding to cloud-free Landsat scenes. Alternatively, a model could be developed for a different sensor that corresponds better with existing datasets. If multiple sensors were used, an atmospheric correction of imagery to remove the combination of light reflected from aerosols might be important in obtaining consistent measurements through time from sensor to sensor. Whether Landsat or another sensor is used, further research should analyze the role that sun glint plays on satellite imagery of Lake Mattamuskeet. A compositing criterion could be used to filter out the observations affected by sun glint.

Remote Sensing vs. Interpolation

Regardless of whether satellite imagery or direct field measurements are analyzed, water clarity is very difficult to predict both spatially and temporally. At any given time, multiple influences are likely acting on the lake's water clarity, extending

from natural occurrences such as storm events to human stressors such as pumping. An activity in one area of the lake may produce unique spatial patterns in that area or elsewhere. Figure 22 is an example of a very high resolution satellite image taken with the DigitalGlobe satellite on January 19, 2014. The image captures the speed at which changes to water clarity are occurring in the lake. Secchi disk measurements performed at the time of this image could feasibly produce a range of values for measurements taken within meters of each other.

In this case, due to the lack of field data corresponding to Landsat scenes and the other influences on radiance measurements such as sun glint, direct interpolations of field measurements were better suited for the habitat suitability analysis. The interpolation comparison results found in this study were similar to results found in previous cases (Murphy et al. 2010). Future analyses could include more variations of each technique, or incorporate additional interpolation methods. The creation of a model using software such as R could allow for a vast amount of iterations using different techniques and inputs. For the scope of this study, it appears that appropriate interpolations for conditions in Lake Mattamuskeet were produced. Given the number of measurements and range of values, the best-performing interpolation techniques in this case did not overwhelmingly outperform the other techniques, suggesting there is some flexibility to which interpolation technique is used.

Habitat Suitability Analysis Scenarios

With sea level rise, it can be expected that the lake level will rise, remaining higher for longer periods of time due to the water control structures remaining closed for longer periods. It might be expected that as lake levels rise, the lake area might increase

laterally, thus increasing the amount of shallow area. In this case, however, impoundments surrounding the lake (particularly along the eastern and southern edges where SAV habitat suitability is highest) prevent the possibility of the lake growing laterally as more water is retained in the basins. Instead, the water will drain into the many smaller canals and impoundments once it has reached its highest possible level. Additional topographic information would be necessary to understand at exactly what point the lake will begin to inundate surrounding land, but clearly due to that lake's connection to the rising Pamlico Sound, depth will increase as long as the topography constrains lateral expansion. In this way, SAV habitat availability will decrease as demonstrated in Figures 14-15. These figures show a decrease in suitable habitat due to an increase in water level. SAV can only grow at depths at which light can still reach it, so this result is expected. More information is necessary to understand how the impacts of climate change and sea level rise will play out physically, but regardless of the rate and magnitude of lake level change, SAV habitat is clearly at risk.

The possibility of managing lake levels was considered here because the reduction of water levels should allow for much more SAV habitat (Figures 14-15). However, the lake is already quite shallow. Further reduction of water levels would reduce the surface area of the lake and potentially, some of the existing SAV habitat. The apparent paradox, that reducing lake levels will produce more SAV habitat, but reducing lake levels will decrease lake surface area and thereby reduce the amount of potential SAV habitat, should be modeled to maximize SAV habitat produced by a range of lake level reductions.

Conclusions

This study successfully located areas for SAV restoration, but also identified a possible threat to SAV habitat in Lake Mattamuskeet. Although sea level rise is a threat to the lake already because the water control structures could be overwhelmed and allow saltwater intrusion, sea level rise and subsequent lake level increases will also reduce available SAV habitat. Restoration may be important to the future survival of SAV in the lake, as it would reestablish SAV where it previously existed. Additional management scenarios, such as the control of lake levels, may be necessary under future conditions to maintain SAV and, in result, improve water-quality conditions in the lake.

This study presents some ideas that can be applied to the management of other coastal lakes with similar water quality conditions and SAV loss. The application of remotely sensed data is a promising approach that, given an initial increase in *in situ* data to develop working models for a given site, might eventually decrease the need for *in situ* data and allow for the study of trends beginning before *in situ* data is available. The habitat suitability analysis portion of this study would be particularly useful to test possible lake levels to improve management decisions regarding lake level and SAV restoration.

References

- Audu, I. and Usman, A. (2015) An application of geostatistics to analysis of water quality parameters in rivers and streams in Niger State, Nigeria. *American Journal of Theoretical and Applied Statistics* **4(5)**, 373-388.
- Burkholder, J.M., Tomasko, D.A., and Touchette, B.W. (2007) Seagrass and eutrophication. *Journal of Experimental Marine Biology and Ecology* **350**, 46-72.
- Butt, M.J. and Nazeer, M. (2015) Landsat ETM+ Secchi Disc Transparency (SDT) Retrievals for Rawal Lake, Pakistan. *Advance in Space Research* **56(7)**, 1428-1440.
- Cho, H.Y. and Poirrier, M.A. (2005) A model to estimate potential submerged aquatic vegetation habitat based on studies in Lake Pontchartrain. Louisiana. *Restoration Ecology* **14(4)**, 623-629.
- Dhillon, J.K. and Mishra, A.K. (2014) Estimation of Trophic State Index of Sukhna Lake Using Remote Sensing and GIS. *Journal of the Indian Society of Remote Sensing* **42(2)**, 469-474.
- Goslee, S.C. (2011) Analyzing remote sensing data in R: the Landsat package. *Journal of Statistical Software* **43**, 1-25.
- Harwell, M.C. and Sharfstein, B. (2009) Submerged aquatic vegetation and bulrush in Lake Okeechobee as indicators of greater Everglades ecosystem restoration. *Ecological Indicators* **9(6)**, s46-s55.
- Havens, K.E. (2003) Submerged aquatic vegetation correlations with depth and light attenuating materials in a shallow subtropical lake. *Hydrobiologia* **493**, 173-186.

- Jensen, J. (2010) *Remote Sensing of the Environment: An Earth Resource Perspective*, 2nd Edition.
- Jeppesen, E., Sondergaard, M., Meerhoff, M., Lauridsen, T.L., and Jensen, J.P. (2007) Shallow lake restoration by nutrient loading reduction—some recent findings and challenges ahead. *Hydrobiologia* **584**, 239-252.
- Kay, S., Hedley, J. D., and Lavender, S. (2009) Sun glint correction of high and low spatial resolution images of aquatic scenes: a review of methods for visible and near-infrared wavelengths. *Remote Sensing* **1**, 697-730.
- Kloiber, S.M., Brezonik, P.L., Olmanson, L.G., and Bauer, M.E. (2002) A procedure for regional lake water clarity assessment using Landsat multispectral data. *Remote Sensing of Environment*, **82**, 38-47.
- Maryland Department of the Environment (2017) Frequently Asked Questions: Chesapeake Bay Water Quality Standards.
<http://mde.maryland.gov/programs/Water/TMDL/Water%20Quality%20Standards/Pages/programs/waterprograms/tmdl/wqstandards/faqs.aspx>. Accessed March 2017.
- Moorman, M.C., Augspurger, T., Stanton, J.D., and Smith, A. *In press*. Where's the Grass? Disappearing submerged aquatic vegetation and declining water quality in Lake Mattamuskeet.
- Mueller, T.G., Pusuluri, N.B., Mathias, K.K., Corelius, P.L., Barnhisel, R.I., and Shearer, S.A. (2004) Map quality for ordinary kriging and inverse distance weighed interpolation. *Soil Science Society of America Journal* **68**, 2042-2047.

- Murphy, R.R., Curriero, F.C, and Ball, W.P. (2010) Comparison of spatial interpolation methods for water quality evaluation in the Chesapeake Bay. *Journal of Environmental Engineering* **136(2)**, 160-171.
- Nelson, S.A.C. Soranno, P.A., Cheruvilil, K.S., Batzli, S.A., and Skole, D.L. (2003) Regional Assessment of Lake Water Clarity Using Satellite Remote Sensing. *Journal of Limnology* **62(1s)**, 27-32.
- NC Coastal Resource Commission (2015) North Carolina Sea Level Rise Assessment Report: 2015 Update to the 2010 Report and 2012 Addendum.
- Orth, R.J., Carruthers, T.J.B., Dennison, W.C., Duarte, C.M., Fourqurean, J.W., Heck Jr., K.L., Randall Hughes, A., Kendrick, G.A., Judson Kenworthy, W., Olyarnik, S., Short, F.T., Waycott, M. and Williams, S.L. (2006) A global crisis for seagrass ecosystems. *Bioscience* **56(12)**, 987-996.
- Ozen, S., Nelson, S., Khorram, S., Moorman, M. and Cakir, H. (2016a) Use of limited data to model lake water clarity from remote sensed data in Lake Mattamuskeet, North Carolina. *Journal of Earth Science Research* **4(1)**, 43-54.
- Ozen, S., Nelson, S., Khorram, S., Moorman, M., and Cakir, H. (2016b) Use of limited data to model lake water clarity from remote sensed data in Lake Mattamuskeet, North Carolina. *Master's Thesis*.
- Pilz, J. and Spock, G. (2007) Why do we need and how should we implement Bayesian kriging methods. *Stochastic Environmental Research and Risk Assessment* **22(5)**, 621-632.

- Poirrier, M.A., Spalding, E.A., and Franze, C.D. (2009) Lessons learned from a decade of assessment and restoration studies of benthic invertebrates and submerged aquatic vegetation in Lake Pontchartrain. *Journal of Coastal Research* **SI(54)**, 88-100.
- Scheffer, S.M., Hosper, S.H., Meijer, M.L., Moss, B., and Jeppesen, E. (1993) Alternative equilibria in shallow lakes. *Trends in Ecology and Evolution* **8(8)**, 275-279.
- Seers, B.M. and Shears, N.T. (2015) Spatio-temporal patterns in coastal turbidity – long-term trends and drivers of variation across an estuarine-open coast gradient. *Estuarine, Coastal and Shelf Science* **154**, 137-151.
- Tango, P.J. and Batiuk, R.A. (2013) Deriving Chesapeake Bay water quality standards. *Journal of the American Water Resources Association* **49(5)**, 1007-1024.
- Tobler, W. (1970) A computer movie simulating urban growth in the Detroit region. *Economic Geography* **46(2)**, 234-240.
- U.S. Department of the Interior, U.S. Geological Survey (USGS 2016a) Landsat 8 (L8) Data Users Handbook. Version 2.0.
- U.S. Department of the Interior, U.S. Geological Survey (USGS 2016b) Landsat Missions Timeline. <https://landsat.usgs.gov/landsat-missions-timeline>. Accessed March 2017.
- U.S. Department of the Interior, U.S. Geological Survey (USGS 2016c) USGS Continuous water-quality monitoring at Lake Mattamuskeet. South Atlantic Water Science Center – North Carolina Office. <https://nc.water.usgs.gov/projects/mattamuskeet/data.html>. Accessed December 2016.

- U.S. Department of the Interior, U.S. Geological Survey (2016). Earth Explorer.
<https://earthexplorer.usgs.gov>. Accessed December 2016.
- Waters, M.N., Piehler, M.F., Smoak, J.M., and Martens, C.S. (2010) The development and persistence of alternative ecosystem states in a large, shallow lake.
Freshwater Biology **55**, 1249-1261.
- Winton, R.S., Moorman, M., and Richardson, C.J. (2016) Waterfowl impoundments as sources of nitrogen. *Water Air Soil Pollution* **227:390**.
- Wu, G., Leeur, Jan and Lin, Y. (2009) Understanding seasonal water clarity dynamics of Lake Dahuchi from in situ and remote sensing data. *Water Resource Management* **23**, 1849-1861.
- Xu, F., Tao S., Dawson, R.W, and Li, B.. (2001) A GIS-based method of lake eutrophication assessment. *Ecological Modeling* **144**, 231-234.
- Zhang, Y.L. Liu, X., Qin, B., Shi, K., Deng, J. and Zhou, Y. (2016) Aquatic vegetation in response to increased eutrophication and degraded light climate in Eastern Lake Taihu: Implications for lake ecological restoration. *Scientific Reports* **6**, 23867.
- Zimmerman, D., Pavlik, C., Ruggles, A., and Armstrong, M.P. (1999) An experimental comparison of Ordinary and Universal Kriging and Inverse Distance Weighting. *Mathematical Geology* **31(4)**, 375-390.
- Zou, W., Yuana, L. and Zhang, L. (2013) Analyzing the spectral response of submerged aquatic vegetation in a eutrophic lake, Shanghai, China. *Ecological Engineering* **57**, 65-71.
- Weather Underground. Weather History for K2DP. Hourly Weather History and Observations. Accessed March 2017.

Table 1. Landsat 8 Bands (modified from USGS 2016a). The Landsat 8 satellite carries two sensors, the Operational Land Imager (OLI) and the Thermal Infrared Sensor (TIRS). The OLI images consist of eight 30-meter spectral bands and one 15-meter panchromatic band. Bands 10 and 11 are collected at 100 meters.

LANDSAT-8 OLI & TIRS BANDS		Wavelength (micrometers)
Band 1	30-m Coastal Aerosol	0.43-0.45
Band 2	30-m Blue	0.45-0.51
Band 3	30-m Green	0.53-0.59
Band 4	30-m Red	0.64-0.67
Band 5	30-m Near-Infrared (NIR)	0.85-0.88
Band 6	30-m Shortwave Infrared (SWIR) 1	1.57-1.65
Band 7	30-m Shortwave Infrared (SWIR) 2	2.11-2.29
Band 8	15-m Panchromatic	0.50-0.68
Band 9	30-m Cirrus	1.36-1.38
Band 10	100-m Thermal Infrared (TIRS) 1	10.60-11.19
Band 11	100-m Thermal Infrared (TIRS) 2	11.50-12.51

Table 2. Band Combinations Tested (from Ozen et al. 2016a). These are the bands and band combinations tested by Ozen et al. (2016a) in the creation of two models using regression analysis to predict Secchi Disk Depth (SDD) from Landsat 8 imagery for the east side and the west side of Lake Mattamuskeet (Eq. 1 and Eq. 2). For the east side, band2+band5 (blue + near-infrared) was the best combination based on the combined lowest Akaike's Information Criterion (AIC), highest r^2 and highest adjusted r^2 (AIC = -111.05, $r^2 = 0.59$, Adj. $r^2 = 0.5$). For the west side, band2+band3+band5 (blue + green + near-infrared) was the best combination (AIC = -101.4, $r^2 = 0.82$, Adj. $r^2 = 0.75$).

Single Band	Band Ratios	Additional Band Combinations
band1	band2/band3	band2+band3+band4+band5
band2	band3/band2	band2+band3+band4
band3	band2/band4	band2+band3
band4	band4/band2	band2+band4
band5	band3/band4	band2+band5
band6	band4/band3	band2+band3+band5
band7	band5/band4	band3+band4+band5
	band4/band5	band3+band4
	band3/band5	band3+band5
	band5/band3	band4+band5
	band5/band2	(band2/band4)+band2
	band2/band5	(band4/band2)+band2
		(band2/band4)+band4
		(band4/band2)+band4
		(band2/band4)+band3
		(band5/band2)+band5
		(band2/band5)+band3
		(band2/band5)+band2
		(band5/band4)+band4
		(band2/band4)+band2+band5
		(band2/band4)+band4+band5
		(band4-band5/ band4+band5)
		(band3-band5/band3+band5)

Table 3. Dates of Available Landsat 8 Imagery. Cloud-free imagery is highlighted, and imagery chosen for the analysis is bolded. The columns are grouped by season, and each bold group of rows represent years.

	Spring			Summer			Fall			Winter		
YEAR	Mar	Apr	May	Jun	Jul	Aug	Sept	Oct	Nov	Dec	Jan	Feb
2013-2014	X	14	16	1	3	4	5	X	8	10	11	12
	X	30	X	17	19	20	21	X	24	26	27	28
2014-2015	16	1	3	4	6	7	8	10	11	13	14	15
	X	17	19	20	22	23	24	26	27	29	30	X
2015-2016	3	4	6	7	9	10	11	13	14	16	1	2
	19	20	22	23	25	26	27	29	30	X	17	18
2016	5	6	8	9	11	12	13	15	16	2		
	21	22	24	25	27	28	29	31	X			

Table 4. Landsat 8 Images Chosen for Analysis. These dates were chosen to represent each seasonal period from 2013-2016. Dates were chosen to include a distributed range of dates and to avoid imagery with cloud interference.

	Spring	Summer	Fall	Winter
2013-14	4/14/13	7/19/13	9/5/13	2/28/14
2014-15	4/1/14	6/6/14	10/26/14	2/15/15
2015-16	5/22/15	6/23/15	10/13/15	2/18/16
2016	5/24/16	6/9/16	9/13/16	12/2/16

Table 5. Summary of SAV Survey Data. SAV presence, depth, and Secchi disk depths measured during 2013-2016 SAV surveys are summarized for the east, west, and lake overall for each year. This summary was used as a basis for assessing the methods to model water clarity and for choosing reclassification values.

Year	LAKESIDE	SAV Presence (%)			Depth (m)			Secchi Disk Depth (m)					
		n	Min	Max	Mean	n	Min	Max	Mean	n	Min	Max	Mean
2013	EAST	64	0	100	71.5781	64	0.254	0.9906	0.7062	19	0.3048	0.508	0.3997
	WEST	38	0	100	12.5789	38	0.1778	1.4224	0.7767	34	0.1778	0.3302	0.2734
	OVERALL	102	0	100	49.598	102	0.1778	1.4224	0.7325	53	0.1778	0.508	0.3187
2014	EAST	63	0	100	29	63	0.3302	1.0922	0.7777	22	0.15875	0.3302	0.2315
	WEST	38	0	95	12.3684	38	0.4064	1.4732	0.9502	13	0.2667	0.4826	0.3282
	OVERALL	101	0	100	22.7426	101	0.3302	1.4732	0.8426	35	0.15875	0.4826	0.2674
2015	EAST	64	0	100	19.9219	64	0.4826	1.2192	0.916	64	0.2	0.5	0.2664
	WEST	38	0	80	7.7632	38	0.381	1.4986	0.926	38	0.2	0.4	0.2737
	OVERALL	102	0	100	15.3922	102	0.381	1.4986	0.9197	102	0.2	0.5	0.2691
2016	EAST	53	0	60	10.2264	53	0.4318	1.4224	0.982	53	0.08	0.3	0.1619
	WEST	51	0	20	0.5882	51	0.5588	1.8288	1.0668	51	0.12	0.25	0.1771
	OVERALL	104	0	60	5.5	104	0.4318	1.8288	1.0236	104	0.08	0.3	0.1693
Overall	EAST	244	0	100	33.709	244	0.254	1.4224	0.8396	158	0.08	0.508	0.2425
	WEST	165	0	100	7.7152	165	0.1778	1.8288	0.9407	136	0.12	0.4826	0.2426

Table 6. Interpolation Comparison. Root mean squared error (RMSE) from leave-one-out cross validation of each interpolation technique for each dataset is shown. The best interpolation methods for each dataset were chosen based on the lowest RMSE (bolded).

Technique		RMSE from Leave-One-Out Cross Validation				
		SAV	2013	2014	2015	2016
IDW	Power = 1	9.67	0.03470	0.04681	0.05989	0.03007
	Power = 2	9.32	0.08856	0.04458	0.06209	0.03050
	Power = 3	9.46	0.08892	0.04456	0.06601	0.03186
Empirical Bayesian Kriging	Power	8.88	0.08685	0.04281	0.05931	0.02839
	Linear	8.94	0.08610	0.04284	0.05944	0.02873
Kriging	Thin Plate Spline	9.40	0.08831	0.04302	0.06131	0.02846
	Ordinary	9.28	0.08786	0.04441	0.06295	0.02843
Global Polynomial	1 st Order	11.7	0.05421	0.05386	0.06827	0.03691
	2 nd Order	10.3	0.04250	0.04108	0.06090	0.03176
	3 rd Order	10.3	0.03422	0.04398	0.06003	0.02985

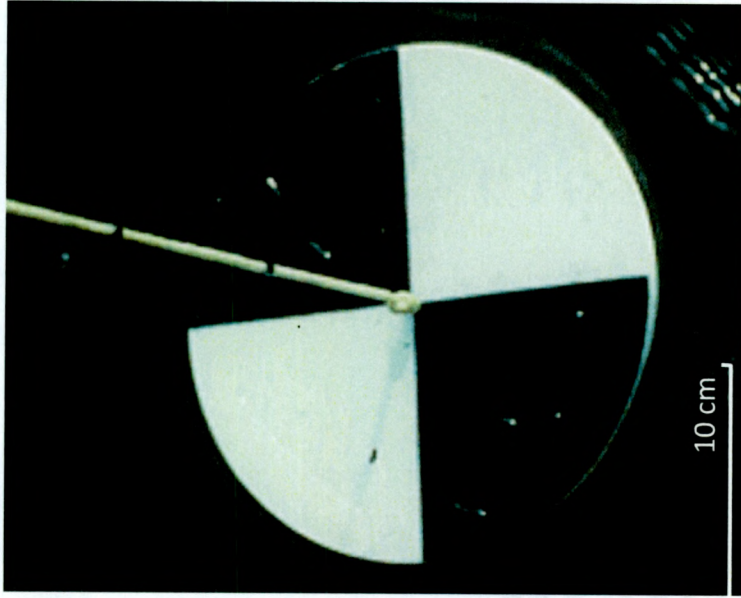


Figure 1. Secchi Disk (from Maryland Department of the Environment 2017). The Secchi disk is 20 centimeters in diameter. It is used to measure water clarity. The disk is lowered into the water and the depth that it can be seen is known as the Secchi disk depth (SDD) or Secchi disk transparency (SDT). The SDD/SDT is approximately equal to one half of the photic zone, the maximum depth of light penetration.

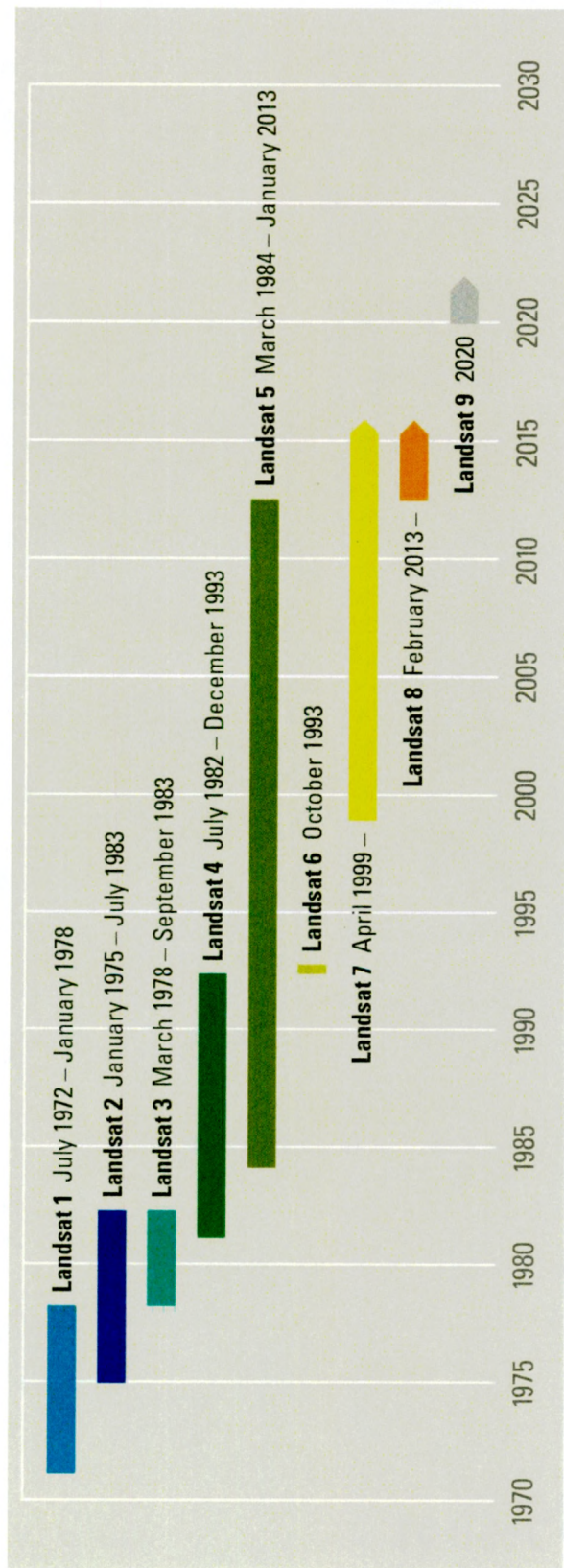
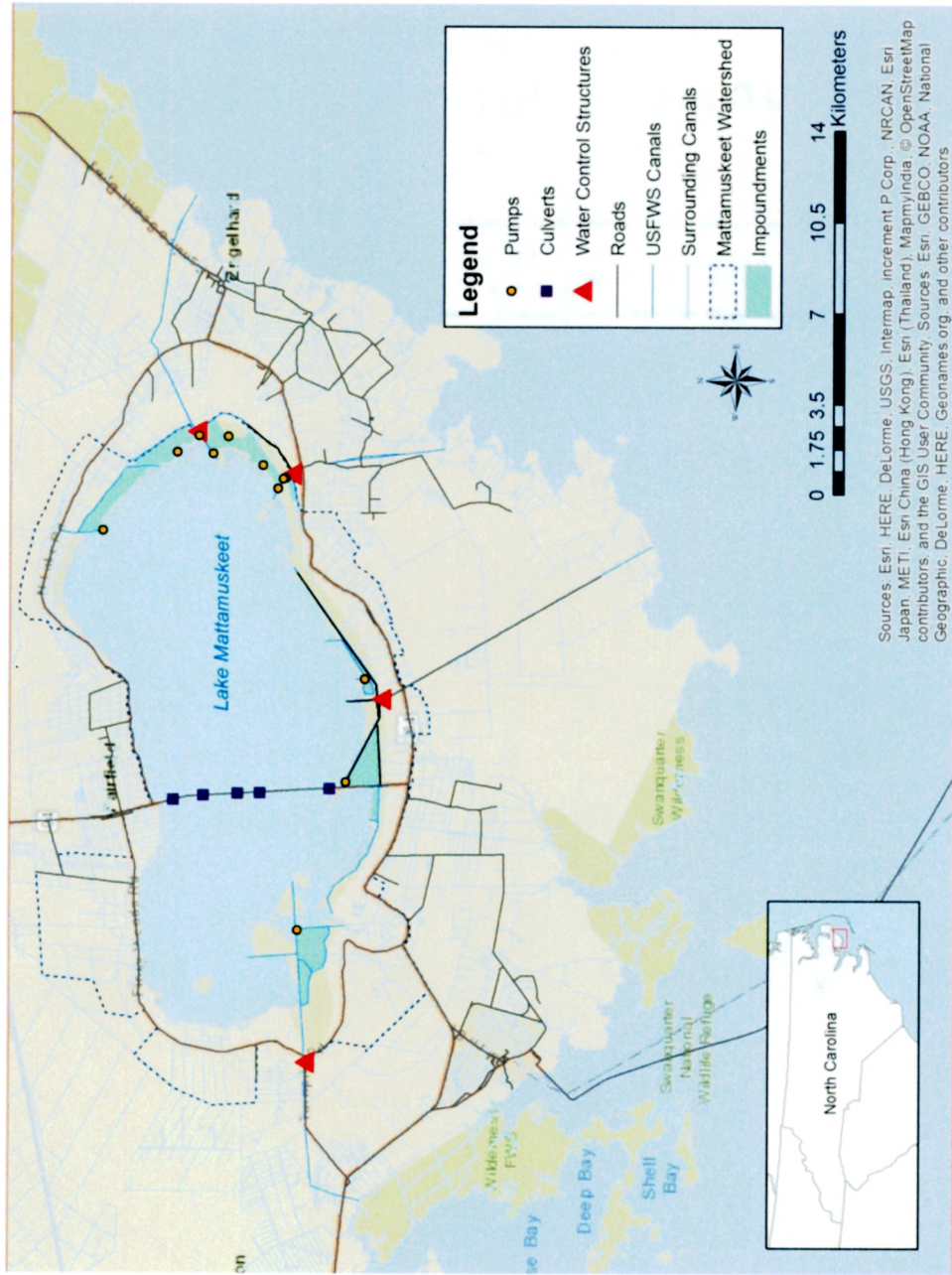


Figure 2. Landsat History (from USGS 2016b). A major benefit of using Landsat for analysis is its long history beginning in 1972 noting that the sensor became advanced with time.



Sources: Esri, HERE, DeLorme, USGS, Intermap, increment P Corp., NRCAN, Esri Japan, METI, Esri China (Hong Kong), Esri (Thailand), MapmyIndia, © OpenStreetMap contributors, and the GIS User Community. Sources: Esri, GEBCO, NOAA, National Geographic, DeLorme, HERE, Geonames.org, and other contributors

Figure 3. Study Site. Lake Mattamuskeet is located on the Coastal Plain in North Carolina. It is surrounded by cropland and a dense network of canals. Four major canals connect the lake to the Pamlico Sound. Water control structures prevent saltwater intrusion but allow water to drain from the lake when lake levels are higher than sound levels. Multiple pumps are used to pump water from impoundments into canals, from which some of the turbid water enters the lake. Only FWS pumps are shown.

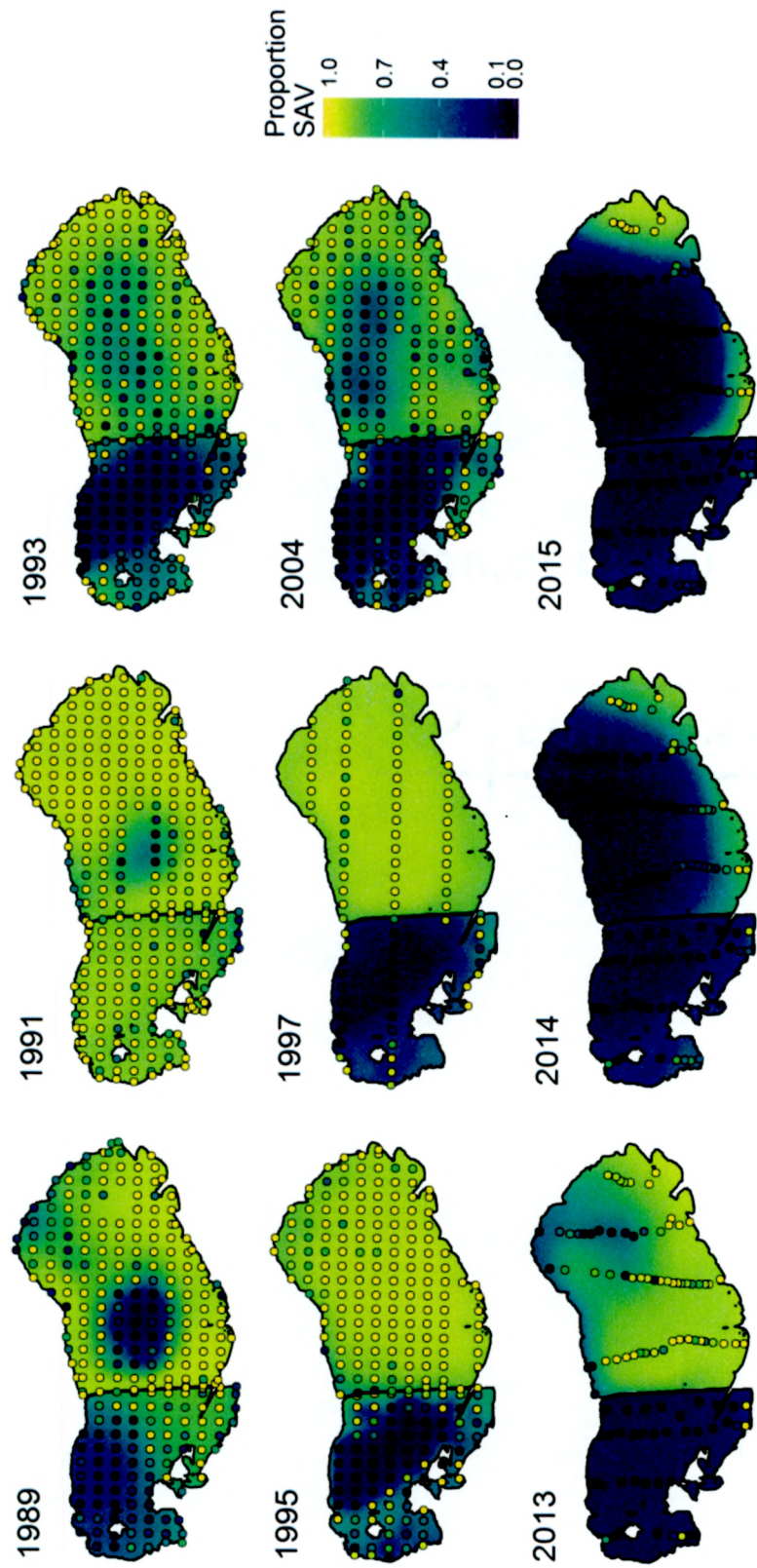


Figure 4. SAV Decline (from Moorman et al. *in press*). These SAV presence maps were produced from SAV survey data and general additive modeling. SAV decline began in the west basin and followed in the east basin in recent years.



Figure 5. Location of USGS Monitoring Stations (from USGS 2016c). Water quality monitors take daily measurements of water quality variables including turbidity.

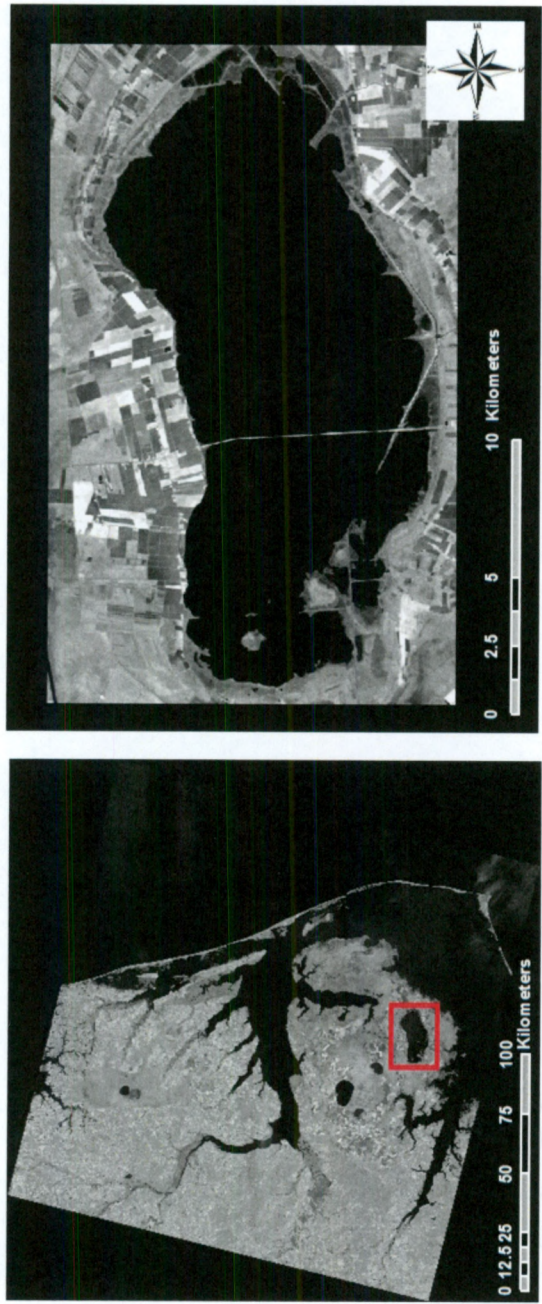


Figure 6. Landsat Scene and Subset. The Landsat scene (path 35, row 14) used for this study (left) and subset (right) to focus on Lake Mattamuskeet. The April 14, 2013 image is shown.

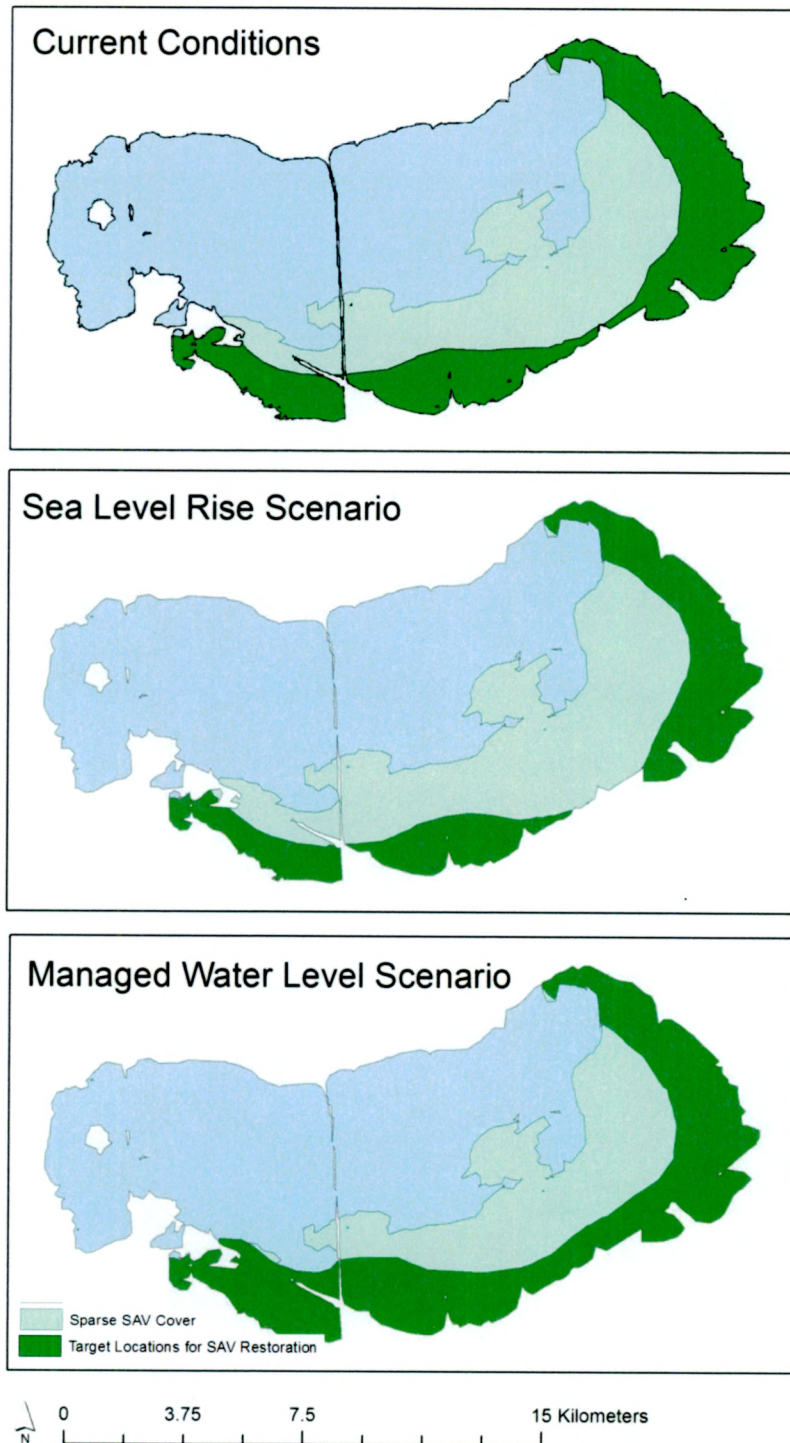
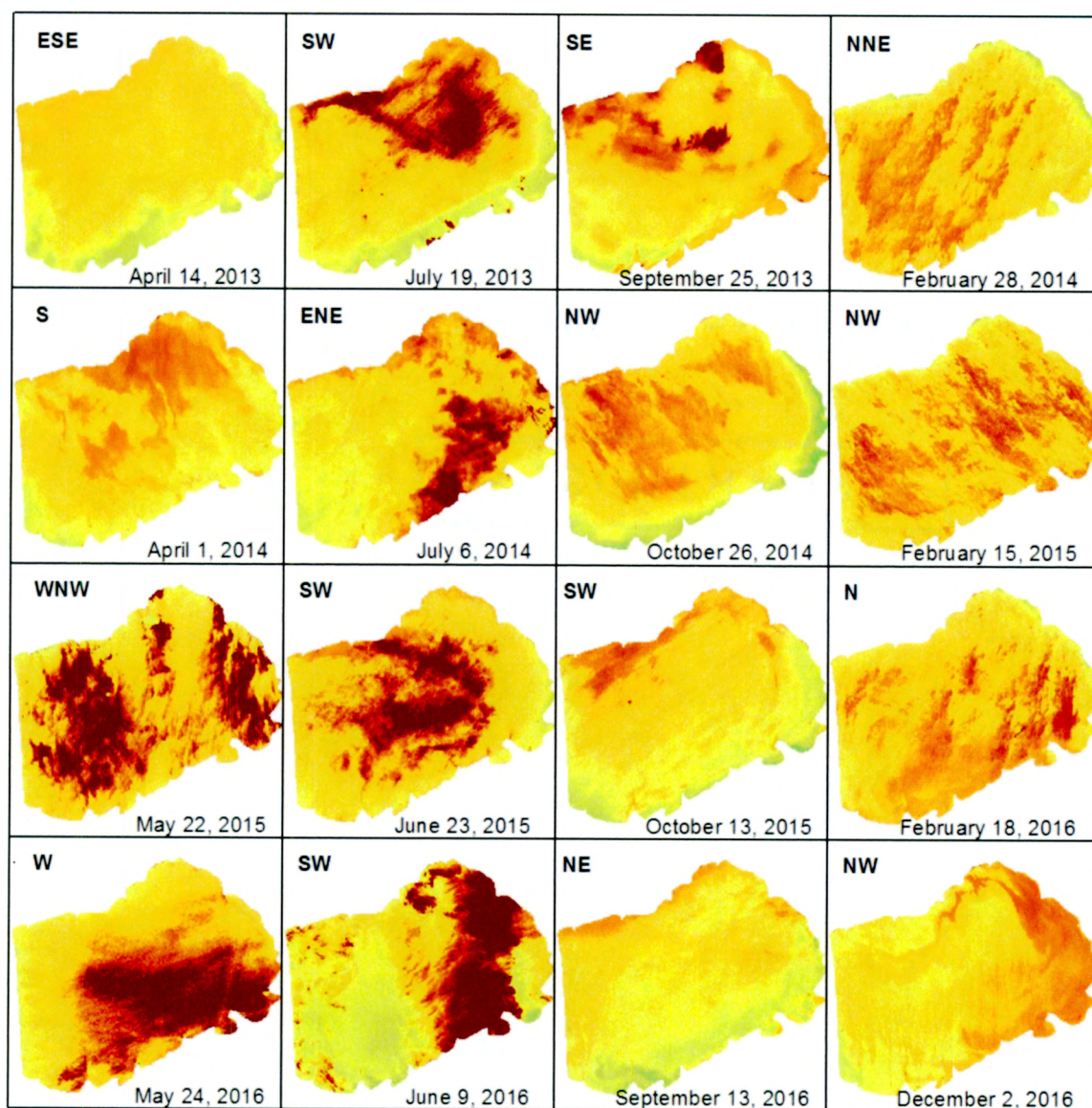


Figure 7. Preliminary SAV Habitat Analysis. Suitable locations for SAV restoration under current conditions and two possible water level scenarios are shown. Sea level rise would cause a decrease in suitable SAV habitat, but managing the lake level to prevent water from continuing to rise would increase the amount of suitable SAV habitat.



0 2.5 5 10
 Kilometers

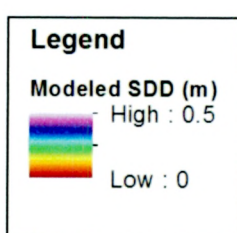
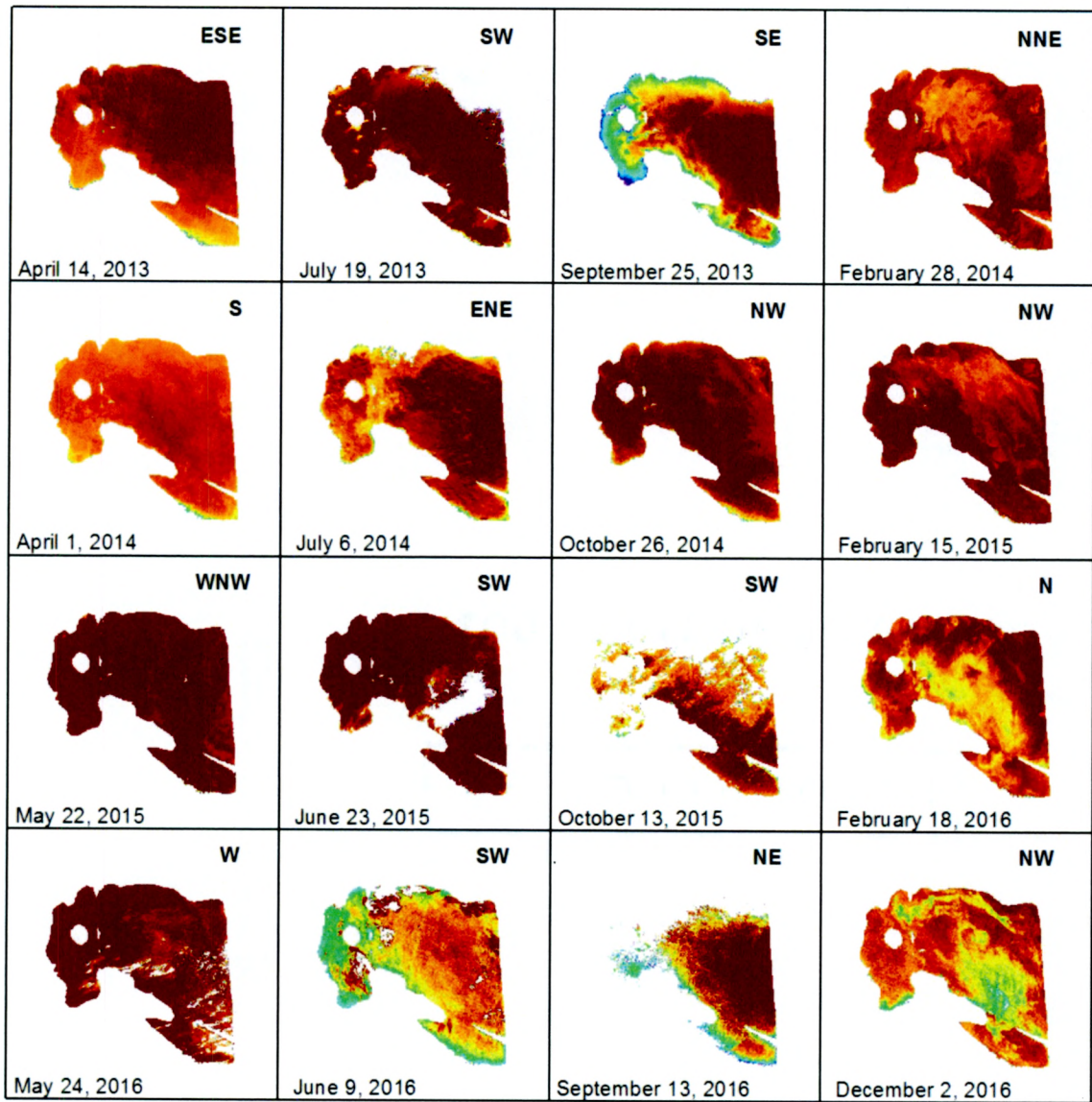


Figure 8. Modeled Water Clarity: East. Output rasters for each Landsat image that was processed for the east side of the lake show that SDD is variable. Extremely low values may be attributed to sun glint (red areas). Overall, the values are lower than expected.



0 2.5 5 10
 Kilometers

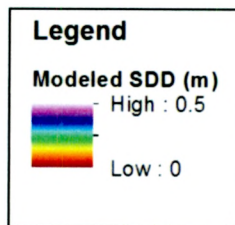


Figure 9. Modeled Water Clarity: West. Output rasters for each Landsat image that was processed for the west side of the lake show that SDD is variable and model results are lower than expected.

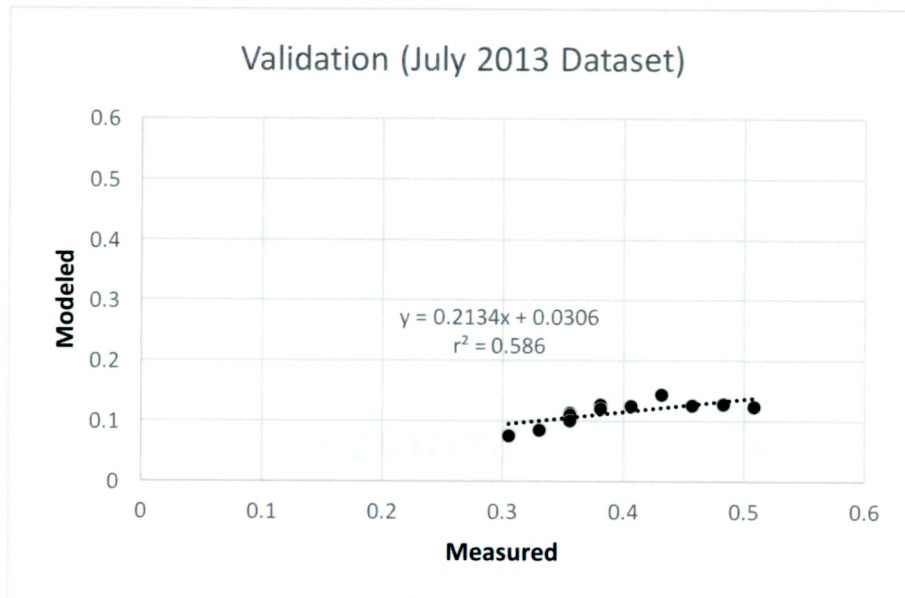
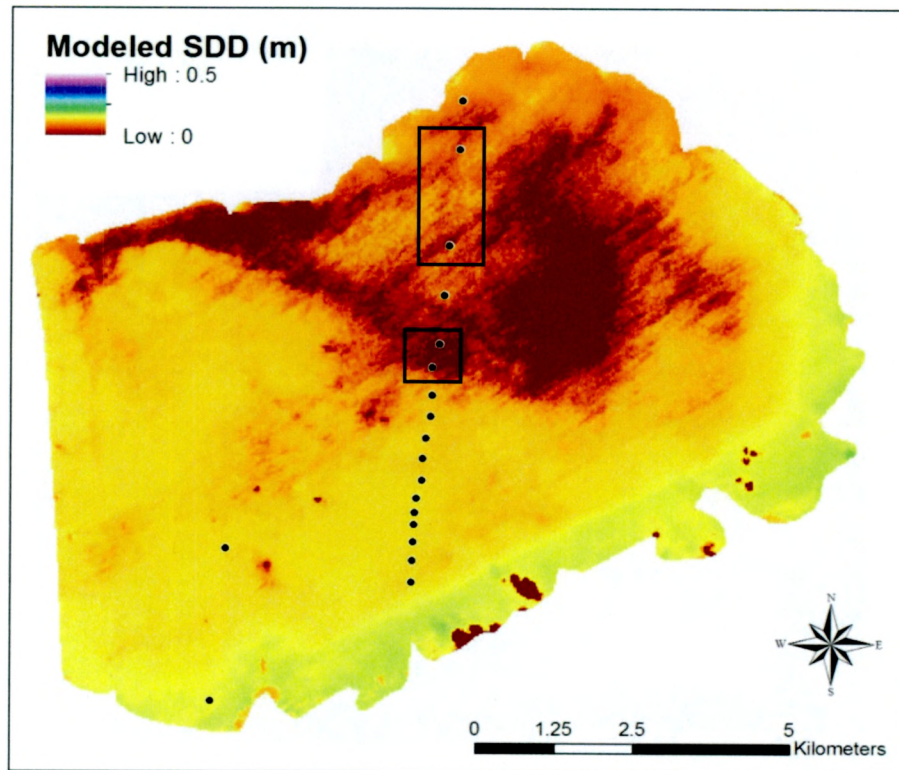


Figure 10. Validation of Water Clarity East Model. For July 2013 field measurements and the July 2013 Landsat image, a relationship was determined between measured and modeled values ($r^2 = 0.58637$). Modeled values are much lower than field measurements. Measurement locations are displayed on the map, and those in black boxes were not used for the valuation because they may have been affected by sun glint. If a 1:1 relationship is forced, the slope is roughly equal to 3.5.

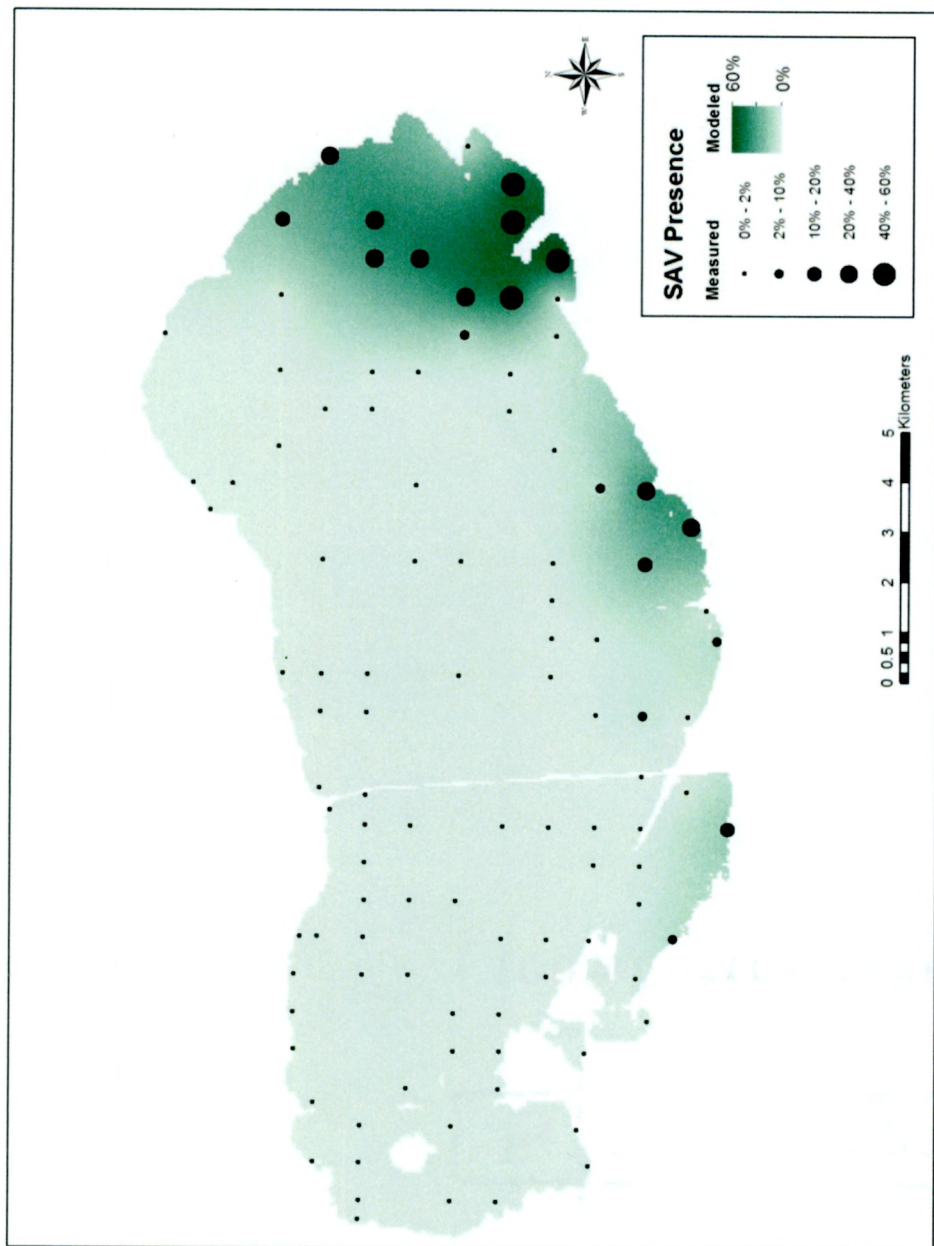


Figure 11 SAV Presence Interpolation. The interpolation for SAV presence is based on the Empirical Bayesian Kriging method and a power semivariogram. Symbol size increases as *in situ* measurements increase, while the light to dark color shows low to high SAV presence according to the interpolated results. Very sparse SAV dominates the lake. The densest areas of remaining SAV occur on the eastern and southern border of the lake.

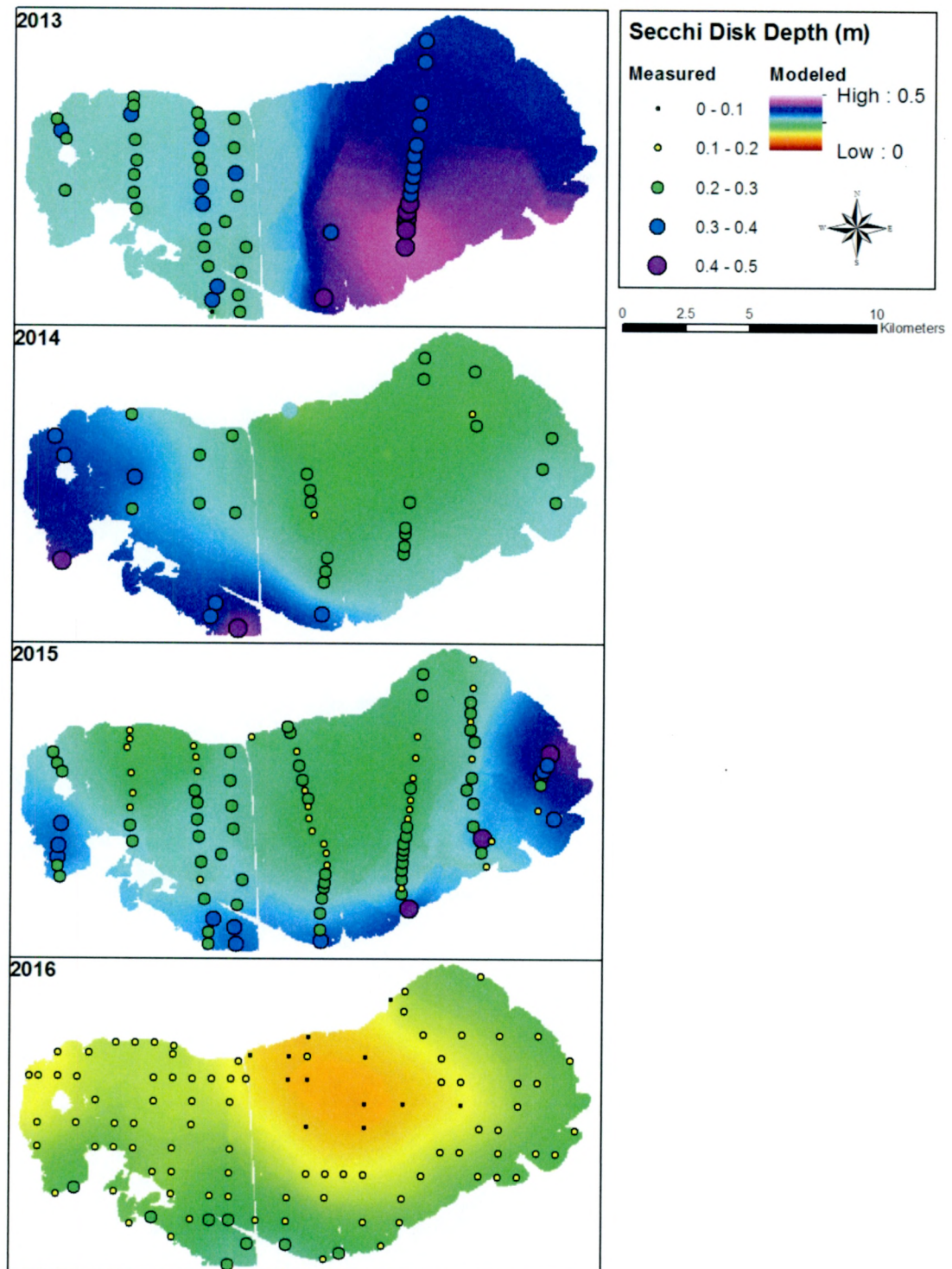


Figure 12. Water Clarity Interpolations. The Empirical Bayesian Kriging technique was the best overall technique for the Secchi disk depth (SDD). The interpolations capture a general decrease in SDD over time. The lack of well-distributed SDD measurements in 2013 caused a wide variation of interpolation results. The IDW technique result is shown for 2013.

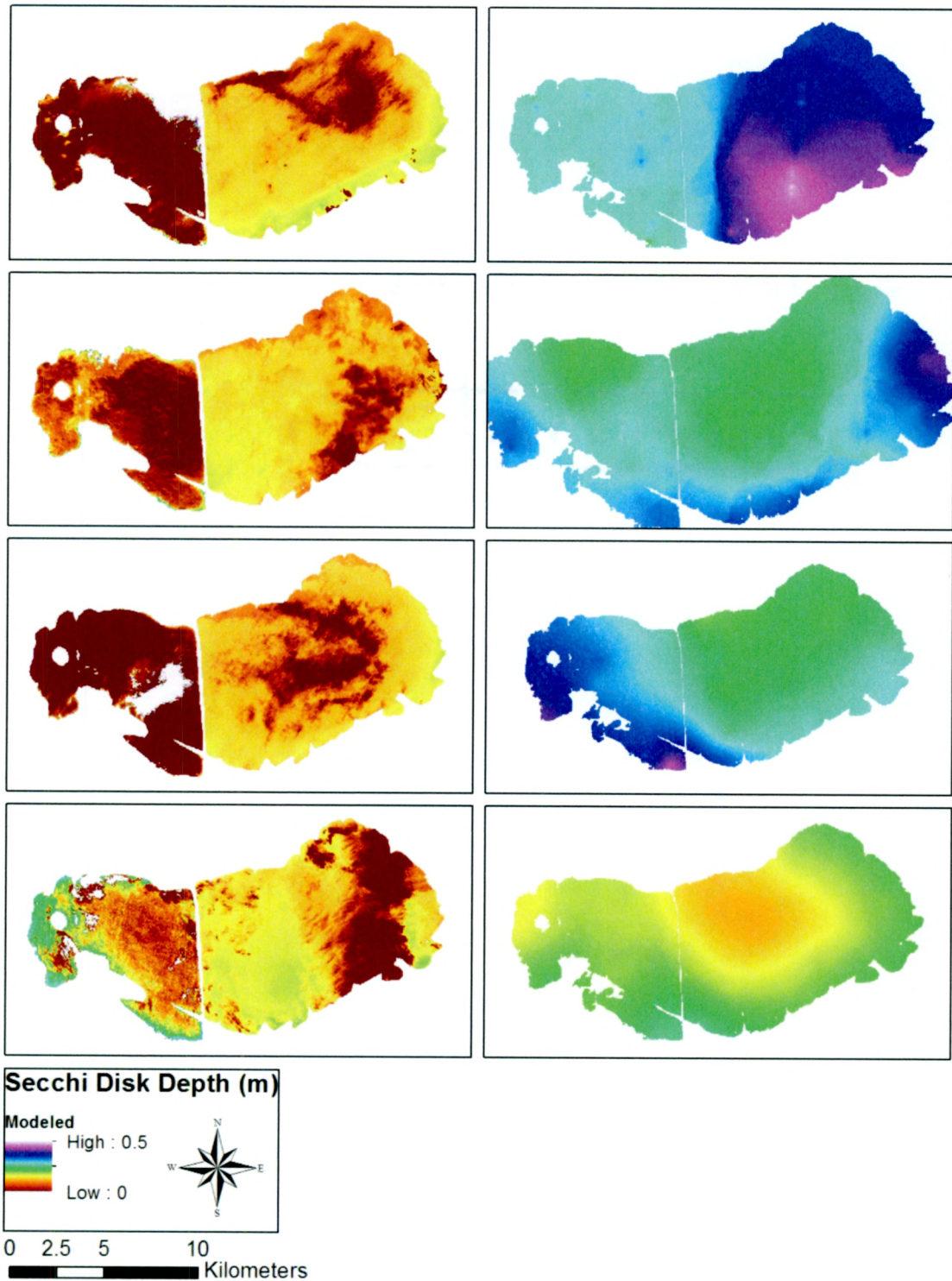


Figure 13. Method Comparison. Output from the remote sensing method (left column) is much lower than output from the interpolation method (right column). Models of summer water clarity are displayed to correspond to the time that the SAV surveys took place.

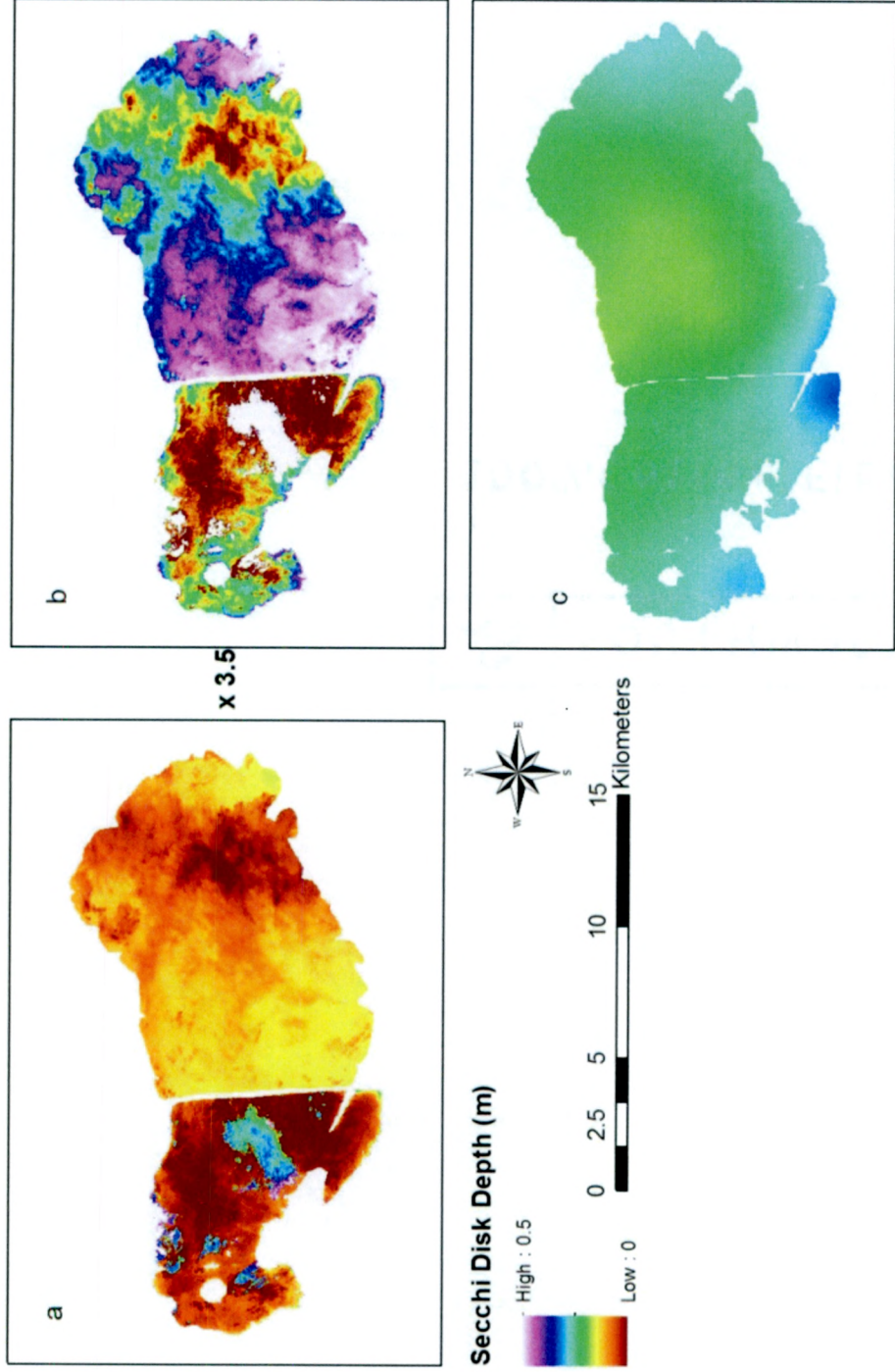


Figure 14. Water Clarity Averages. The mean of the summer 2014, 2015, and 2016 output from the remotely sensed model (a) and the interpolations (c) was calculated. The 2013 results were omitted from the interpolation methods because the interpolation was highly variable, and then omitted from the remote sensing average in or der to created two comparable outputs. The remote sensing average was multiplied by a factor of 3.5 to correct model output to realistic values (b).

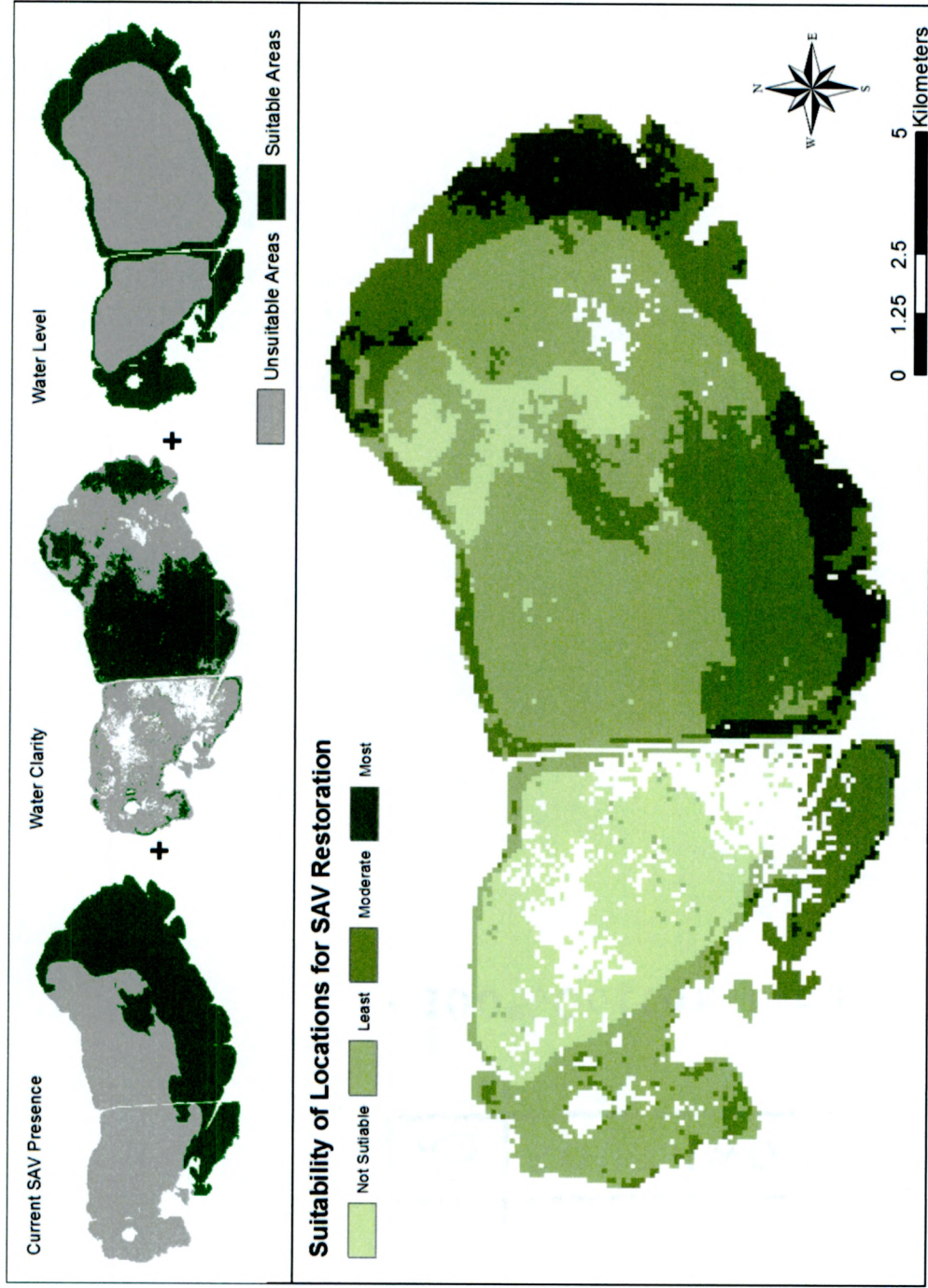


Figure 15. Target SAV Restoration Locations, Remote Sensing Methodology. Three final rasters representing SAV presence, water clarity, and water level (top row) were used to find the most suitable locations for SAV restoration.

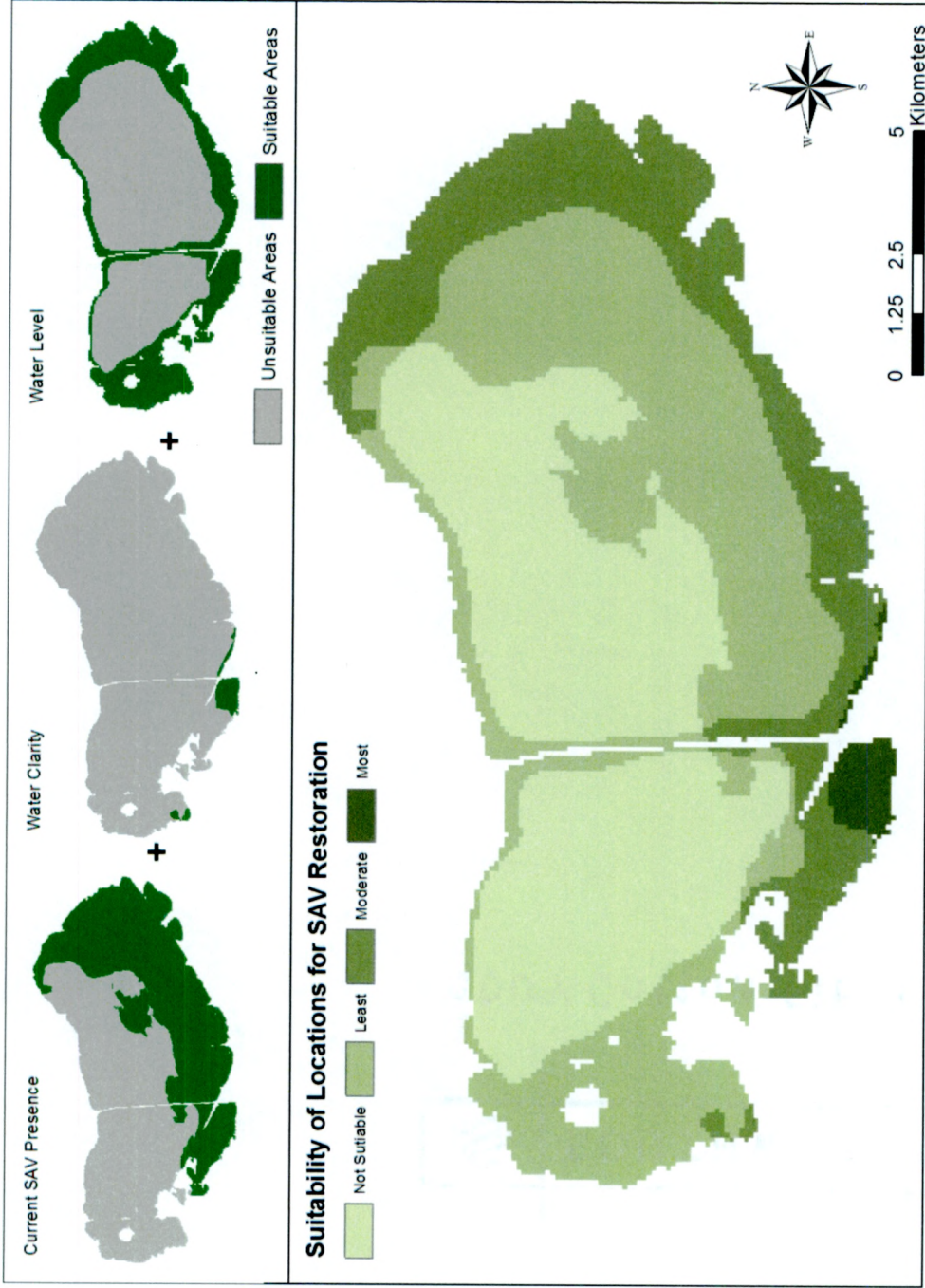


Figure 16. Target SAV Restoration Locations, Interpolation Methodology. Three final rasters representing SAV presence, water clarity, and water level (top row) were used to find the most suitable locations for SAV restoration. Suitable water clarity takes up the smallest area in the lake and is the limiting parameter for the analysis.

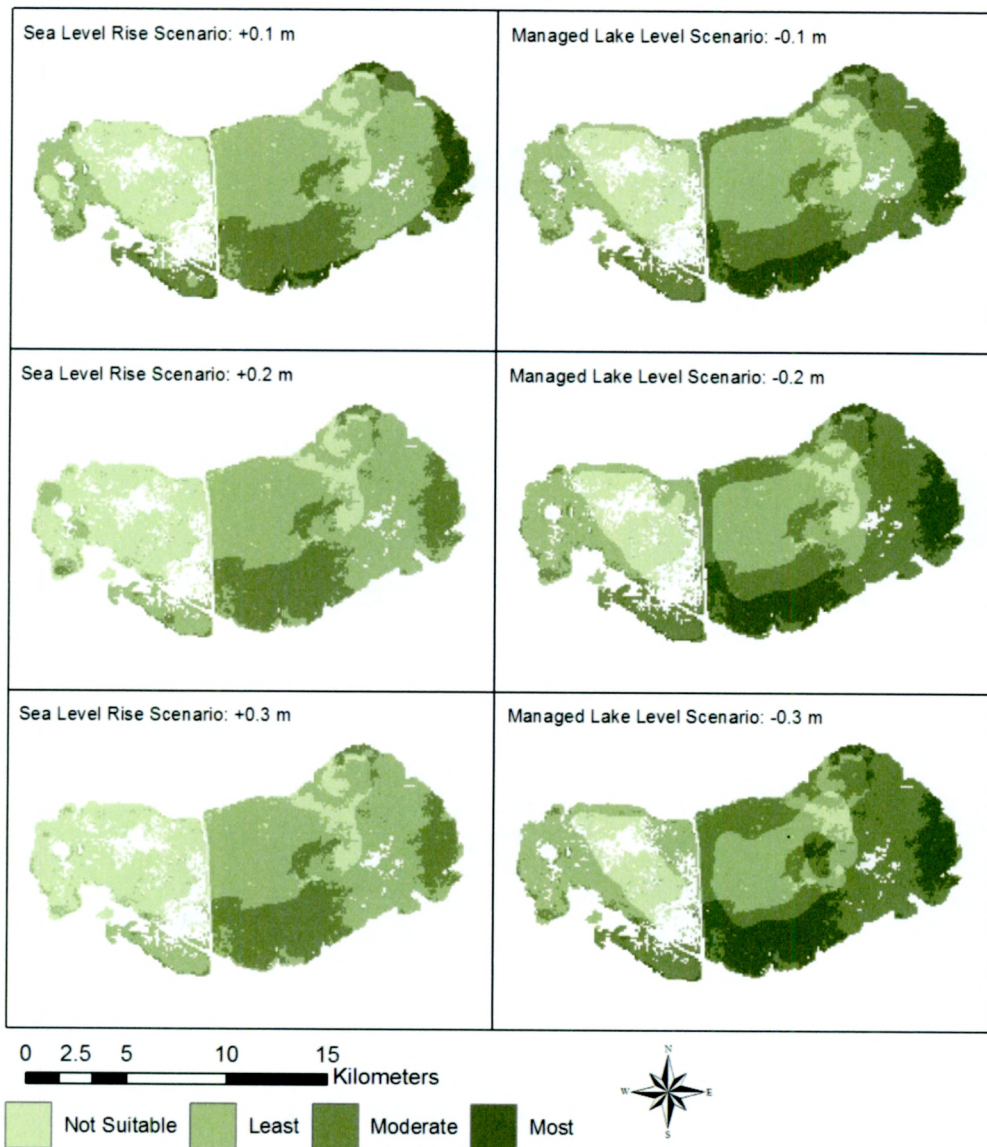


Figure 17. Initial Condition Variations, Remote Sensing Methodology. The same habitat suitability analysis was performed for various sea level rise and managed lake level scenarios. The left column shows a decrease in water level, and the right shows an increase in water level at 0.1 meter increments. Although the most suitable area available does not change severely because it is limited by water clarity, changes in depth impact the available moderately suitable habitat.

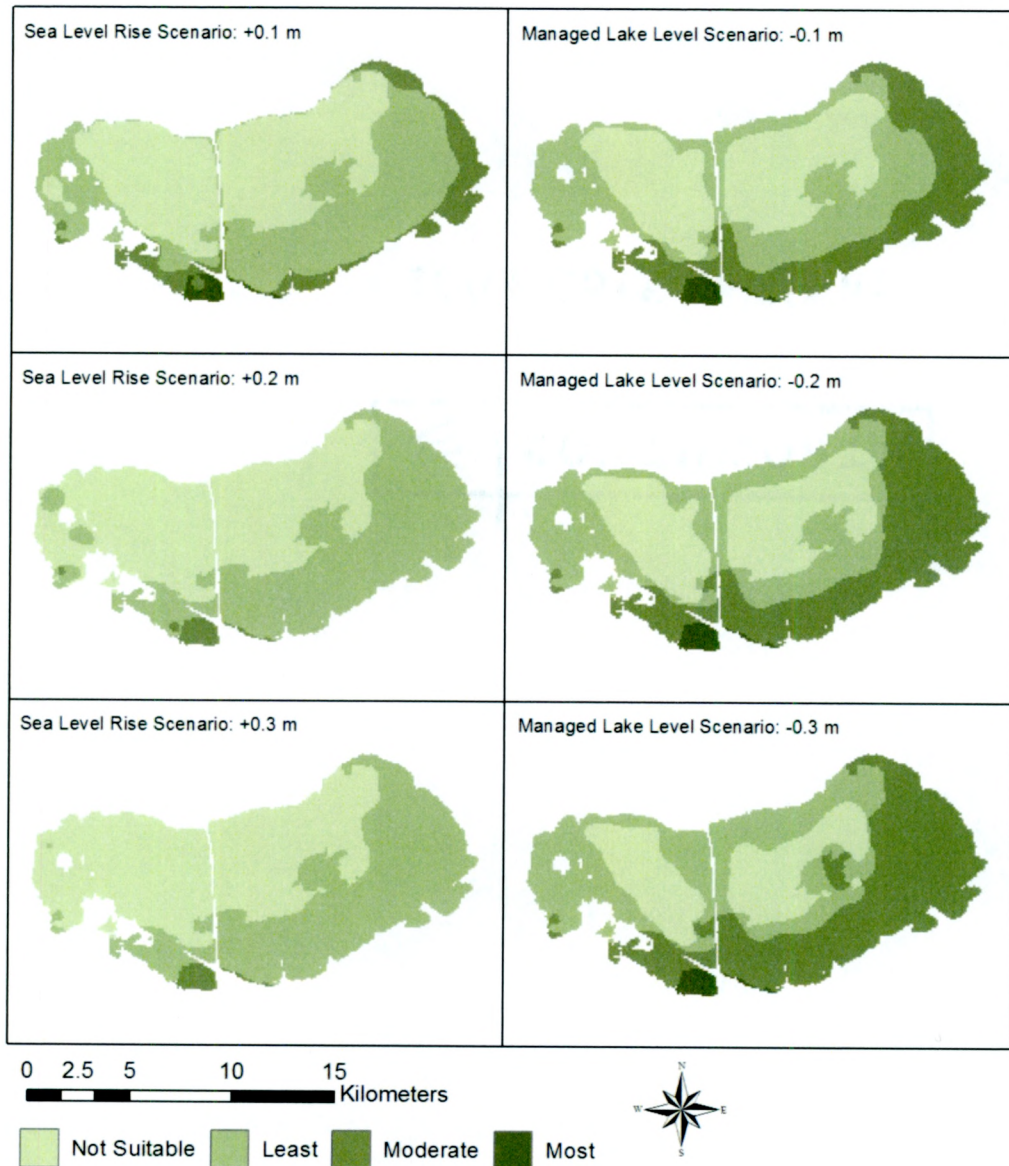


Figure 18. Initial Condition Variations, Interpolation Methodology. The same habitat suitability analysis was performed for various sea level rise and managed lake level scenarios. The left column shows a decrease in water level, and the right shows an increase in water level at 0.1 meter increments. Although the most suitable area available does not change severely because it is limited by water clarity, changes in depth impact the available moderately suitable habitat.

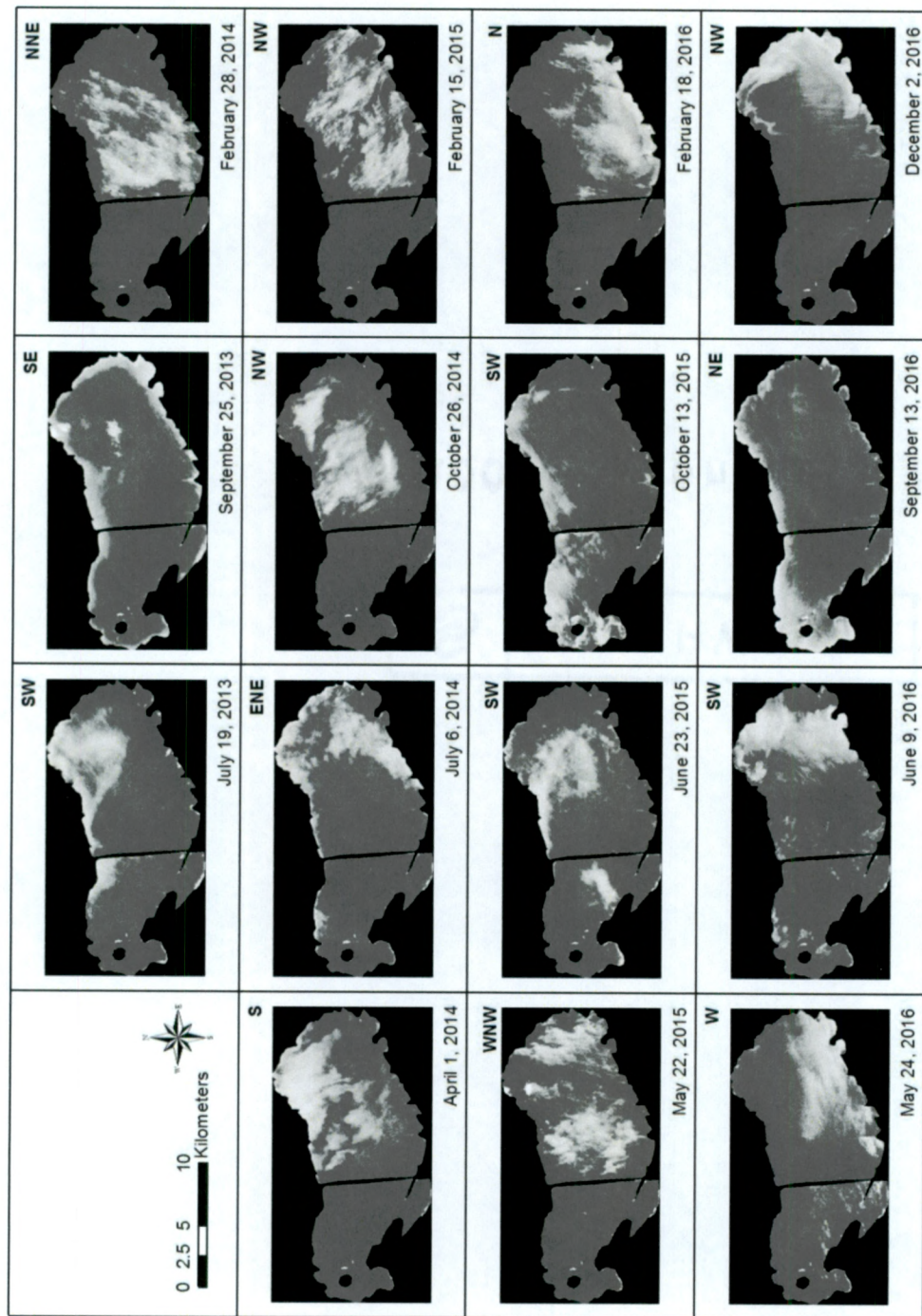


Figure 19. Near-Infrared Band of Images After Histogram Matching. The histogram for each band was shifted to match the histogram for the April 14, 2013 band (not pictured). Reflectance is high in areas with linear patterns that correspond to wind direction (top right corners), which may depict wind-driven ripples. Reflectance observed in the NIR band over water is an indicator of sun glint.

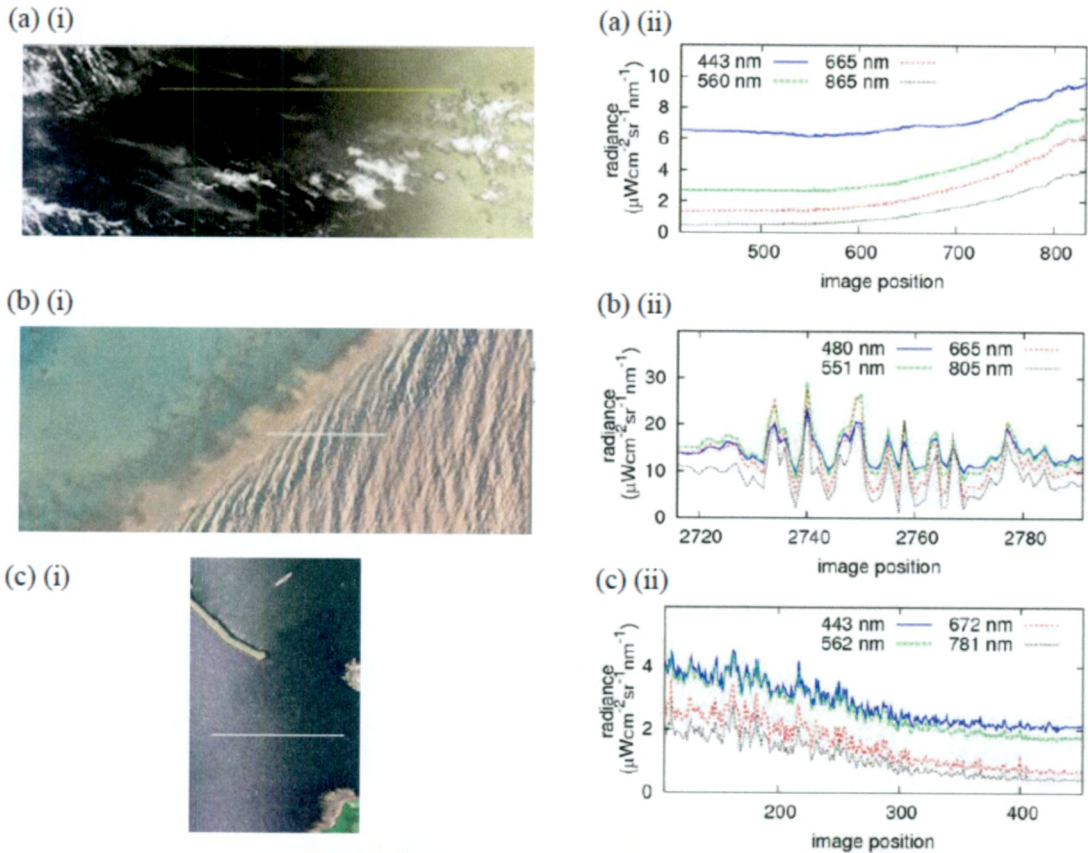


Figure 20. Examples of Sun Glint (from Kay et al. 2009). The left column shows examples of imagery impacted by sun glint and the right column shows radiance along the transect shown in each image. The areas with glint show higher radiance. The pattern appears to be different in each image. Image (b) is impacted by waves, similar to observations of Lake Mattamuskeet.

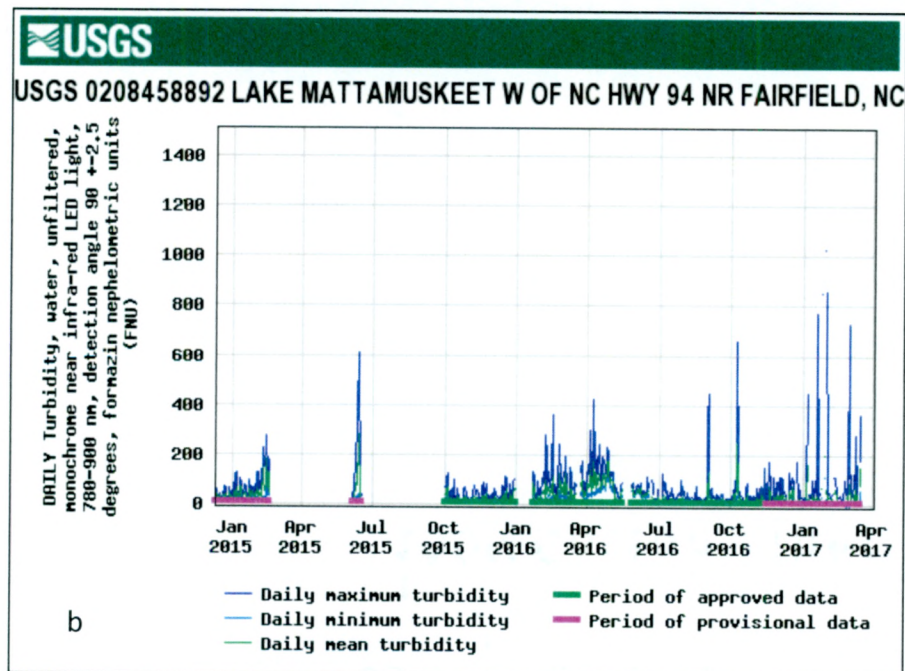
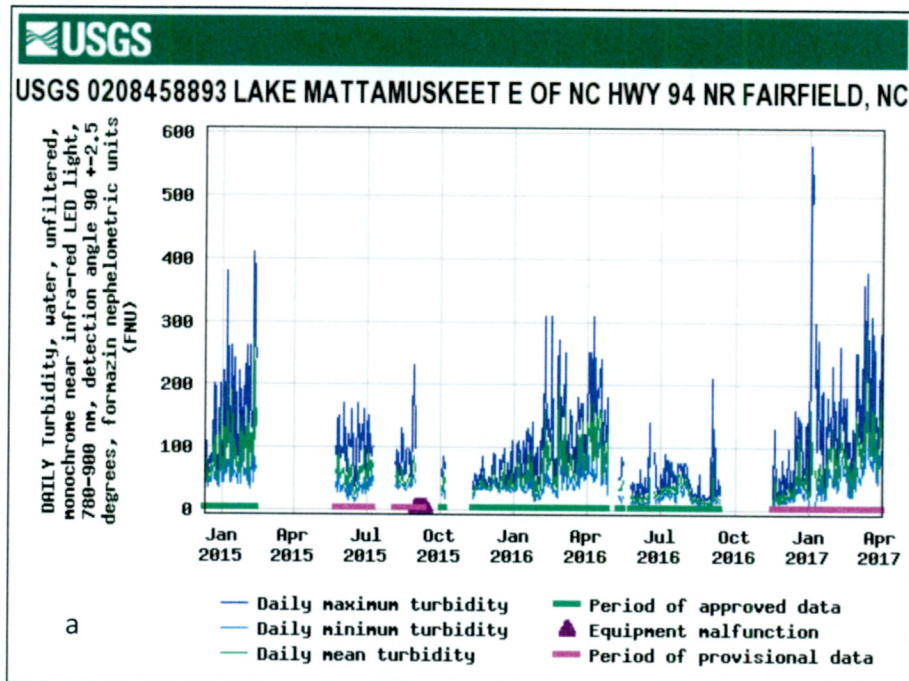


Figure 21. Turbidity Trend in Lake Mattamuskeet (from USGS 2016c) Turbidity in the east (a) and wet (b) from USGS Monitoring Station daily measurements. The green line, depicting mean turbidity, peaks in late winter/early spring. It is lowest in the summer and fall. Spikes in maximum turbidity are typically, but do not always occur in both sides of the lake at the same time. They occur at various times in the year, suggesting high variability, possibly during weather events.



Figure 22. High Variability of Water Clarity (from Google Earth 2017). The DigitalGlobe Satellite Image of Lake Mattamuskeet shows a portion of the southern border of the lake near where Route 94 bisects it. In this small section of the lake, clouds of sediment appear in the water column. The cloud of sediment shows how quickly water clarity can change in the lake both temporally and spatially. The sediment appears to have crossed through the southernmost culvert from the east to the west side of the lake, showing that, though the two sides may need to be analyzed separately, the conditions in the two sides impact each other. The image also depicts the surrounding cropland, which may also contribute nutrients and sediment to the lake.